Study and Analysis of Gas Barrier Properties of 2D WS_2 (Tungsten Disulfide) Nanosheets based PET (Polyethylene-terephthalate) Membranes

By

Muhammad Salman Shah

School of Chemical & Materials Engineering

National University of Sciences & Technology

2022

Study and Analysis of Gas Barrier Properties of 2D WS_2 (Tungsten Disulfide) Nanosheets based PET (Polyethylene-terephthalate) Membranes

Name: Muhammad Salman Shah

Reg. No: 00000319897

This thesis is submitted as the partial fulfillment of the requirements of the

degree of

MS in Chemical Engineering

Supervisor Name: Dr. Sarah Farrukh

School of Chemical and Materials Engineering

National University of Sciences and Technology

H-12, Islamabad, Pakistan

September, 2022

Dedication

I dedicate this work to my parents and without their unflinching support it would not have been possible

Acknowledgements

ALLAHAMDOLILLAH! Thanks to the King and owner of Dominion, ALLAH Almighty who has always been Most Benevolent, Most Merciful and Most Loving. Thanks to ALLAH for blessing me the health, ability, energy and aptitude for this and all the works throughout my life.

I would like to thank my supervisor **Dr. Sarah Farrukh** who has a major contribution in completing mt research and whose guidance and support throughout the course of my research proved very valuable for me. A best mentor, supporter, teacher and above all a matchless supervisor. Her belief in me and my ability always motivated me and kept my morale high. Her navigation helped me to get through all the hardships. All the efforts and cooperation she did during this research, I am forever indebted to her for that.

I would like to express my gratitude to my GEC members **Dr. Erum Pervaiz** and **Dr. Sofia Javed** for their help and guidance in every step of the way.

I would like to thank all the faculty, lab engineers, lab attendants and every single person of SCME for support, without it was not possible.

I'm extremely grateful to **Mr. and Mrs. Muhammad Ikram Qureshi**, my father and mother, thanks a ton to them for always being there to support me in every aspect whether it was moral, financial or any possible way. It can never be compensated. Thanks a lot, to my siblings, for assistance and guidance to achieve this milestone. I would like to thank my brother **Engr. Muhammad Inam Abbas** for guiding me, making my work technically sound. Thanks for always being a backup.

I'd like to express my deepest thanks to **Umaima**, my friend, for limitless support throughout research. Her help always motivated me and led me to productive and remarkable solutions technically and emotionally during my research.

I would like to thank all the family members and friends for their immense moral support from beginning to the end.

Abstract

Science and technology never stop to flourish for ease of human being. Packages materials are very important and frequently used product. Passing time brings different type of issues. An issue is reported worldwide, leakage of Carbon Dioxide gas through voids of PET (Polyethylene Terephthalate) bottles in beverages industry. Advancement of science and technology drove researchers to work for advance materials, 2D nanomaterials have splendid properties which can be helpful to get through this industrial issue. Variety of layered structures materials are available on planet earth as a gift of nature. Tungsten Disulfide (WS_2) is a novel material with splendid properties to build barrier for gas. 2D nanosheets of WS_2 can be incorporated in polymer to overcome gas leakage. Different scientific approaches are applied in laboratories and process industries to get desired form of a materials. Synthesis of 2D materials have different methods. In this study 2D nanosheets were synthesized by Liquid Phase Exfoliation. Which were incorporated in industrial PET by using TIPS (Temperature Induced Phase Separation) method. Different samples were prepared on the basis of variation in two factors, Centrifuge RPM and loading of nanosheets (weight percent). Nanosheets were synthesized on three different values of centrifuge RPM 500, 750 and 1000 RPM. Nanocomposites were prepared with four different values of filler loading 0.0024, 0.005, 0.01 and 0.02 weight percent. 700 RPM and 0.01 weight percent of filler appeared to be the best value after comparison of results. Thin films of PET/WS_2 nanosheets were tested by gas permeation testing unit, remarkable reduction in CO_2 was observed. Experimental findings were compared to theoretical models, it was discovered that the Cussler model came the closest to our experimental findings. SEM, XRD and AFM techniques were used to authenticate the study. Morphology and porosity were confirmed by SEM, for analytical measurements AFM technique was used and XRD proved the crystallinity of nanosheets and presence of nanosheets in polymer structure.

Table of Contents

List of Figure

List of Table

List of Acronyms

PET Polyethylene Terephthalate

NMP N-methyl-2-Pyrollidone

WSNS Tungsten Disulfide Nanosheets

DMT Di Methyl Terephthalate

OTR Oxygen Transmission Rate

TIPS Temperature Induced Phase Separatio

Chapter 1

Introduction

1.1. Background

Science and technology never stop to work in alignment with needs of human being. Passing time have increased demand of packing materials as it's a matter of fact that every product whether its food or any other thing requires packing. Food industries specially needs a lot of variety in for packing materials depending upon the product specifications. Plastic bottles are widely used in beverages and pharmaceutical industries. We have variety of materials and polymers used to make plastic bottle along with fillers and colors. One of the most visible effects of urbanization has been a change in the industrial sector toward PET packaging, particularly in the carbonated beverage sector. CO_2 level from PET bottles drop after some time due to permeation through walls [1]. Plastics production increased from 15 million tons to 311 million tons in 50 years after launching of PET in packages but with a flaw [2]. Flaw is the various permeability characteristics [3, 4]. CO_2 leakage reduces the shelf life and the flavor decreases [5]. The inherent issue of PET is the finite permeability characteristics which limits its use [6]. PET polymer usage has been abundant in bottle manufacture, and its market continues to develop due to its excellent qualities. Traditional materials such as metals (aluminum cans) and glass bottles have recently been replaced by PET polymer for the aforementioned applications due to cost effectiveness, ease of production, light weightiness, and unbreakable properties. J. Rex Whinfield and James T. Dickson of England held the first PET polymer preparation patent, claiming to have produced a synthetic polymer with useful but uncommon qualities that could be utilized to make textile fibers and filaments [7]. Following the first PET bottle patent [2] plastics production skyrocketed for the next 50 years, rising from 15 million tons in 1964 to 311 million tons in 2014, and is expected to double again in the next 20 years, with plastic packaging accounting for 26 percent of total volume of plastic used [8]. While there are numerous advantages to using PE0020T there is one significant disadvantage to using PET bottles: their finite gas permeability characteristics [9] [10] [11]. While packaged

beverages with low gas and vapor permeation rates have a longer shelf-life [12], this inherent issue limits the use of PET for packaging in this context [13]. PET's O_2 barrier characteristics are insufficient to provide a reasonable shelf life unless stored at refrigeration temperatures. Also, CO_2 levels in carbonated beverages fall over time due to absorption through the walls [14], which reduces overall flavor [15].

The lowering of gas permeability can be utilized to extend the shelf life of carbonated beverages. The International Society of Beverage Technologists defines beverage shelf life in terms of CO_2 loss, with storage period equivalent to 17.5 percent loss of CO_2 for soft drinks and 10% loss of CO_2 for beer. The evaluation of shelf life in the beverage sector is a critical issue; in the case of carbonated soft drinks, estimating the loss of carbon dioxide or the external oxygen entrance via the walls has proven a difficult task. The shelf life of a carbonated drink is heavily reliant on the resistance provided by the polymeric container walls to gas molecules attempting to diffuse through them. Furthermore, PET has been found to be more permeable to oxygen than glass, resulting in stalled drinks owing to oxidation. Carbon dioxide levels in drinks decrease over time due to permeation through the walls, and if the level falls below 15%, the drink becomes stale and has a flat taste. Taste degradation is also associated with bottle transparency because it allows easy access to sunlight, which aids the degradation process. A loss of 15% carbonation in 90 days is regarded acceptable for a two-liter bottle, limiting the storage time to nine months, however a 250mL bottle has a far shorter storage time, i.e., 2-3 months. [16]. Gases are the major component of different food and biomedical products. Moisture and gas barrier are main concerns in food packages. Loss of specific component from the substance packed may result to a total difference in the quality i.e CO_2 leakage from sift drinks results in waste of product. Plastics production increased from 15 million tons to 311 million tons in 50 years after launching of PET in packages but with a flaw [2].] Enhancing gas barrier properties is a hot topic for scientists and engineers. Enhancing PET gas barrier properties is far better then replacing PET by glass or metallic packaging material, due to its cost efficiency and recycling properties

1.2. PET (Polyethylene Terephthalate)

PET is a long chain thermoplastic polyester that has been extensively used in beverages industry due to its inertness which results in retainment of taste and prevents food contamination, unbreakable characteristics and light weightiness which allows it to be easily transported and ease of production are some of its excellent characteristics which make it very attractive polymer in beverage industry. Inadequate gas barrier properties result in contamination and staleness of beverage before time, hence the need for its composites with improved properties is imperative. Its crystallinity varies from amorphous to crystalline, thin pet films are transparent whereas thicker films have opaque appearance. Because most variations of PET are semi-crystalline with a major crystalline portion, its melting point (Tm) ranges between (250-260)°C, as does its intrinsic viscosity (IV), which is also a measure of its molecular weight, bottle grade PET has IV ranging from (0.75-0.85)dL/g, and because it also contains amorphous regions, its glass transition temperature (Tg) ranges from (67-81)°C PET exhibits semi-rigid PET Polyester fibres have been utilised in a wide range of applications, and the majority of the world's PET output is for synthetic fibres (more than 60%), with bottle manufacture accounting for roughly 30% of worldwide demand. In the late 1950s, PET was created and employed as a film in a variety of applications, including video, photographic, and X-ray films, as well as flexible packaging. Later, PET was modified and strengthened with micro fillers such as mica and glass, which gave PET the dimensional stability required for injection moulding and extrusion. PET was stretched by blow moulding, stress blow moulding techniques, and the first oriented three-dimensional structures such as bottles were manufactured from the PET in the early 1970s. This advancement resulted in the widespread usage of PET as a lightweight, durable, chemically inert packing material with reasonably good gas barrier qualities.

1.3. PET Preparation

PET can be produced using two methods: transesterification and esterification. The former involves a reaction between an ester and an alcohol, whereas the latter involves a reaction between a carboxylic acid and an alcohol.

Transesterification: It's also called as DMT method (Figure 1), it involves the heating and melting along with stirring of DMT (Di-Methyl-Terephthalate) at 150-160^{o}C in an inert environment containing nitrogen, heated DMT is then reacted, stirred and heated at 150-200^{o}C with ethylene glycol transesterification reactors at normal pressure under nitrogen atmosphere, the methanol produced is continuously removed via distillation which serves as a driving force for the reaction, the reaction occurs in the presence of basic catalysts namely metal oxides, amines, alkoxides, acetates etc., with their concentration ranging from 0.01-0.1wt%. Product from transesterification reactors is transferred to polycondensation reactor, excess ethylene glycol from previous reactor is distilled by a gradual increase in temperature to 250^{o}C at normal pressure, followed by polycondensation that involves reduction in pressure to <1mbar and a rise in temperature to around 270^{o}C-280^{o}C for higher molecular weight polymer. This reaction too proceeds under the presence of catalysts, frequently used are germanium, antimony, lead compounds and titanium at a miser concentration of 0.005-0.05wt%.

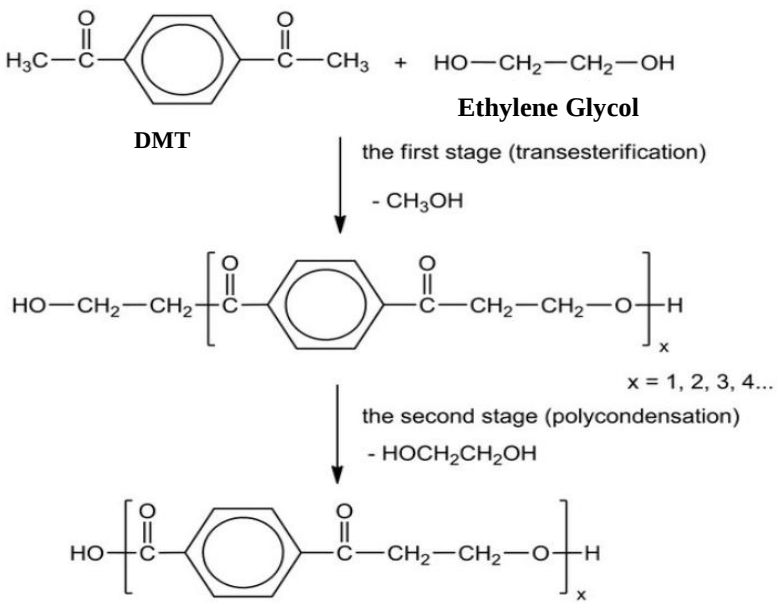

Figure 1 PET Manufacturing Process Transesterification

Esterification: This method (Figure 2) involves the direct esterification of Terephthalic acid with ethylene glycol, its preferred over transesterification process because of its high

reaction rate, no catalyst requirement and results in higher molecular weight PET. Direct esterification is performed in the 220^{o}C-260^{o}C temperature range and (2.7-5.5) bar pressure range with water being continuously removed via distillation, the reaction could also be accelerated using amines if needed, gradual pressure along with temperature increase follows direct esterification in addition to distillation of excess ethylene glycol, the next step is polycondensation that proceeds the same as in transesterification process.

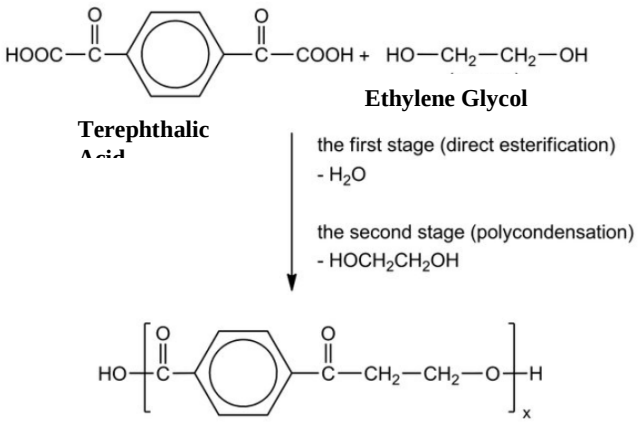

Figure 2 PET Manufacturing Process- Esterification

1.4. WS_2

Tungsten disulfide is a highly chemical and thermal resistant compound of Tungsten and Sulfur having crystalline form. WS_2 have hexagonally arranged tungsten layer between two layers of sulfur. Layers are held together by Van Der Wall forces which indicates that its easy to make thin layers of WS_2. Its black in color. Its melting point is close to 1250^{o}C and it is 2D semiconductor (electronic property)

WS_2 have various applications in industries such as ligt emittors, photovoltaic and in preparation of polymer composites for gas barrier properties.

WS_2 has a layered structure similar to graphite with Tungsten and Sulfur atoms bonded covalently in a single layer and weakly bonded with interlayer weak van der waal forces that makes the separation of a single layer(exfoliation) feasible when subjected to ultrasonication, named as WSNS (Tungsten Disulfide Nanosheets).

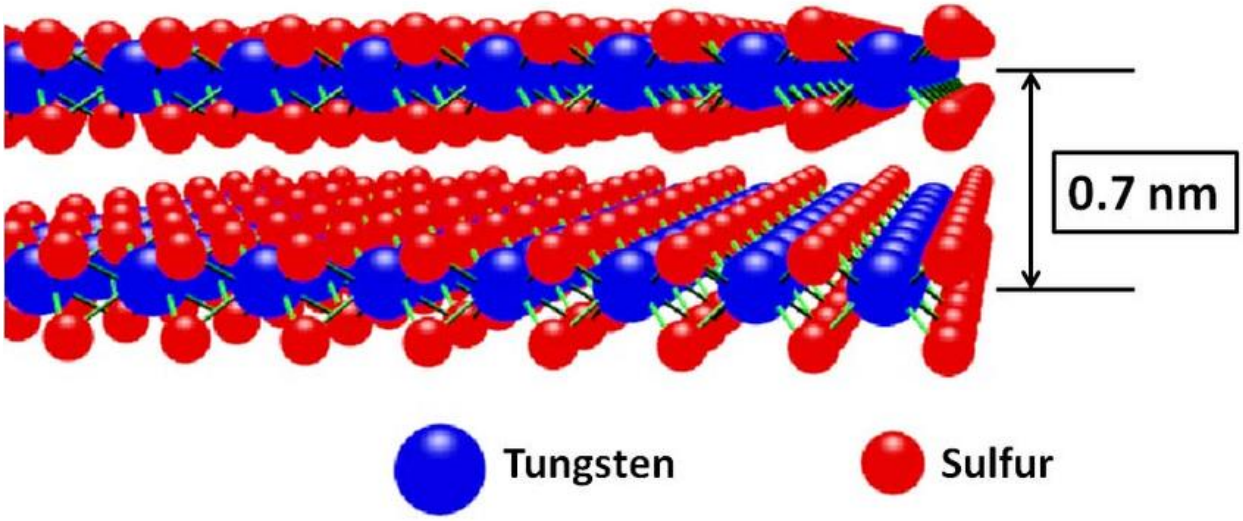

Figure 3 Tungsten DiSulfide

1.5. Liquid Phase Exfoliation

Layered materials with strong in-plane covalent bonding and weak out-of-plane van der waal bonding can be split into a single layer with a thickness in the nanoscale range. This process of separating mono or few layers from their bulk precursor is known as delamination or exfoliation. The most common method of exfoliating nanolayers is liquid phase exfoliation, which involves the use of a solvent. Liquid phase exfoliation is accomplished through ultrasonication, which involves the transfer of high frequency sound wave energy to the liquid samples. When sonic energy is applied to the liquid sample, solvent molecules begin to oscillate at the frequence. During this process, sound waves go through compression and rarefaction cycles, causing solvent molecules to move towards and away from each other. During the rarefaction cycle, solvent molecules move apart and exceed the critical molecular distance that keeps a liquid intact, generating cavities or bubbles. The cavities or bubbles formed collapse at the end of each rarefaction cycle, releasing a large amount of energy in the form of a shock wave. Because a significant amount of energy is generated during this process, the sample must be kept cool by utilizing a cooling bath. PET bottles are readily used for manufacturing of packaging materials for various industries i.e., Beverages medicines and chemicals. Intact gases within the bottles are compulsory to retain the properties of the product. As a matter

of fact, every innovation has pros and cons, so as PET bottles have. Industrialists and scientist are taking it seriously. Therefore, gas barrier properties of PET must be enhanced to get rid of this issue

1.6. Need for WS_2-PET Nanocomposites

High aspect ratio and biocompatible characteristics of WS_2 nanosheets make them an ideal candidate for utilization in beverage industry where gas leakage from bottles is a recurring issue. Considering their high aspect ratio, WS_2 incorporation into polymer would result in enhanced gas barrier properties without affecting other vital parameters, namely, chemical inertness and transparency.

1.7. Outline of Thesis

The **first** chapter introduces the issue and explains how and why PET became the go-to polymer for the beverage industry following its discovery. PET manufacturing procedures are also detailed, as are the advantageous qualities of PET and its gas barrier property, which limits its extensive applicability. Boron Nitride and its qualities are also discussed, as well as how it may aid in strengthening PET's intrinsic gas barrier capabilities.

The **second** chapter discusses all of the research that has been done so far in the current field. It provides an in-depth look at all of the fillers that have been utilized to improve the gas barrier qualities of PET through the blending approach.

The **third** chapter is focused on the materials used for fabrication of PET-WS_2 nanosheets nanocomposite films and the synthesis techniques used. It further includes the characterization techniques employed for characterizing the prepared samples such as SEM, AFM, Tensile strengths and XRD.

The **fourth** chapter comprises the results of permeation testing and comparison of experimental work with the theoretical models. SEM, AFM Tensile Strength and XRD results are also discussed in detail.

The **fifth** Chapter summarizes the present work and the **sixth** chapter includes recommendations for future.

Chapter 2

Literature Review

Polymers and polymer composites have different synthesis methods and various application. Tremendous work has been done previously which shows the importance of polymer nanocomposites.

2.1. Need of WS_2

Conventionally 0D (silica nanoparticles), 1D (carbon nanotubes) and 3D (segregated graphene nanoplatelets) materials were used for different industrial applications such as electronics, sensors, biomedical, etc. But over the past decades 2D materials got attention due to their marvelous properties of 2D nano-plane, bio compatibility, bio degradability, thermal conductivity and gas barrier [17, 18]. There are different types of 2D materials such as graphene, molybdenum disulfide (MoS_2), tungsten disulfide, hexagonal boron nitride (h-BN) etc. The discovery of graphene in 2004 caught splendid attraction towards 2D materials due to its high thermal conductivity, protective coating, and gas barrier properties. Graphene is a single layer of graphite (simplest allotropic form of carbon) having hexagonal crystalline structure. It is used for variety of applications in the field of electronics, sensors, biomedical and membrane technology. [19] [20]. Although graphene exhibits extensive properties but it does not show a bandgap (minimum energy needed for an electron to set free from its bound state) as compare to other 2D materials [21]. Commercially graphene has low production due to high cost. The dispersibility and compatibility of graphene in polymers is poor. Hydrophobicity and agglomeration are the other two properties which bring graphene to lower priority among the other 2D materials [22]. Novel 2D materials have replaced graphene due to their unique properties in various fields such as catalysts, photovoltaic devices, optics and sensors [23]. Researchers are now focusing on such 2D materials due to their high specific surface area and aspect ratio. Until now different number of 2d materials have been discovered. For example, transition metal dichalcogenides (TMDs), Layered double hydroxides (LDHs), h-BN and transition metal oxide (TMOs). Such materials are in the form of ultrathin sheet like structure [24].

Recently 2D nanosheets due to their layered structure and high aspect ratio got substantial attention for many applications, such as in gas separation, gas barrier, energy storage, electrochemical devices, proton conduction and solar cells. The exposed surface atoms and active sites of such 2D nanosheets are really high due to their thin layered structure [25]. 2D nanosheets display high potential to interact with polymer by electrostatic attraction, physical adsorption, van der Waals force and hydrophobic interaction. The blend of 2d nanosheets with polymer improves the separation and barrier properties, biocompatibility and mechanical strength [26, 27]. We have different number of 2D nanosheets discovered for instance borocarbonitrides, hexagonal boron nitride, graphene, montmorillonite and MoS_2, WS_2 and h-BN [28]. Among all these 2D nanosheets, MoS_2 is one of the most significant material due to its low cost, robustness, high abundance and exceptional activity [29]. MoS_2 layered structure material which have weak out-of-plane interactions and strong in-plane bonding, because of these two it shows tremendous chemical, mechanical and physical properties [30]. MoS_2 is used for cocatalysts to provide best cost-effectivity and efficient hydrogen photocatalytic production because of unsaturated Sulphur (S) atoms along with the affinity to proton (H^+) in solution [31]. Nowadays, researchers are heading towards enhancing the gas barrier performance by adding MoS_2 nanosheets into different polymers. This combination has shown a lot of potential in the enhancement of different properties for various applications. MoS_2 due its superior properties, shows promising results in membrane technology [32]. In the earth's crust, tungsten (W) is a less expensive, less dangerous, and more common metal than molybdenum. This family's heaviest transition metal is W, and its larger size can be exploited to adjust characteristics. Today, WS_2 has become a research-attractive side. Pure WS_2 layers are not magnetic. The bulk semiconductor WS2 is more stable against oxidation and heat than MoS_2 and has an indirect band gap (1.3 eV). [33]. The indirect semiconductor is transformed into a direct semiconductor when it is converted from bulk to monolayer form. straight one with a 2 eV band gap. WS_2 monolayers are identical to MoS_2 monolayers in terms of electronic and structural properties. Monolayer WS_2 has distinct properties, such as high emission. Maximum spin-orbit coupling, high binding energy, non-blinking emission, and quantum yield. The straight band gap of WS_2 allows for visible fluorescence. WS_2 monolayer. WS_2 has a large field of view when compared

to other TMD's good effect mobility thermal stability, band structure. Tungsten disulfide is a well-known TMD with intriguing properties, their reinforcing capacity in polymer matrices has received less attention than that of other transition metal dichalcogenides members such as MoS_2. Furthermore, no reviews of tungsten disulfide based polymer nanocomposites published. As a result, the focus of this review is on WS_2-based polymer composites. Many scientists have newly become interested in WS_2-based polymer nanocomposites, and the use of tungsten disulfide as a nanofiller is rapidly growing due to developments in strength along with thermal qualities.

2.2. Structure of WS_2 nanosheets.

As previously stated, tungsten disulfide is a highlighted member of the transition metal dichalcogenides family, with a layered structure comparable to hexagonal MoS_2 (2H). It's difficlut to differentiate between (W)tungsten and (Mo)molybdenum dichalcogenides since their structures are so similar. Strongly bonded SWS sandwiches are found in the 2D structure of tungsten disulfide, whereby inplane bonding is used to snack tungsten(W) atoms between Sulfur(S) layers. WS_2 nanosheet can be divided in 2 vairants based on the arrangement of Sulfur atoms: trigonal prismatic 2H (D3h) and octahedral 1T (Oh). Two phases have different properties, such as 2H is semiconducting and 1T is of metallic. The carrier concentration in the 1T phase is higher, but the thermal conductivity is lower. The inter-layer atomic glide, however, permits convenient conversion of a phase to another, and when gliding, one of the S-planes is displaced. Two layers are stacked in a trigonal prismatic geometry with hexagonal symmetry in the 2H unit cell. The weak van der Waal interactions aid layers to stack together in this trigonal prismatic form. The 2H polytype of tungsten disulfide crystal lattice belongs to the nonsymmetric hexagonal space group P63/mmc (D4 6h). The unit cell of WS_2 is stretched over two layers in the 2H polytype, with the S atoms of the second layer on top of the W atoms of the starting layer and vice versa. The z-parameter is used to determine the relative locations of the S atom, which are found to be 0.6225. Because of the limited carrier concentration, broad band gap in the semiconducting 2H phase causes low electrical conductivity. Blending with other conductive fillers such as graphene, metal nanoparticles, and carbon nanotubes (CNT) can negate this effect. Tetragonal symmetry

and octahedral co-ordination of metal atoms are common in octahedral phases. The W atoms are coordinated in an octahedral way in the 1T form of WS_2 [34].

To get an ABC stacking arrangement in 1T, the S layers are typically displaced in comparison to other designs. The band gap of semiconducting WS_2 in bulk is between 1 and 1.5 eV, and it is an indirect band gap. The magnetic, optical, and electrical characteristics of monolayers are all good than those of the bulk. In the development of one layer WS_2, an interesting transition from indirect to direct band gap may be seen. Variations in band structure as thickness of WS_2 decreases have important applications in a variety of sectors. In WS_2, the WW bond length is 3.15, which is the same as the MoMo bond length (3.16) in MoS_2. However, with WSe2 (3.28), this parameter is slightly greater. The main difference among Mo and W based chalcogenides is scale of the spin–orbit coupling, which develops owing to size differences. A rhombohedral form of WS_2 (3R) structure, which is isotypic with the 3R form of MoS_2, was also defined in supplement to hexagonal structure [35].

2.3. Synthesis of WS_2 nanosheets

Bulk WS_2 is used as an intercalation material and lubricant in rechargeable batteries. Field effect transistors , energy storing devices , optoelectronic devices, photodetectors, sensors, and catalysts can all benefit from the conversion of bulk material into some layered structures [36]. TMD qualities can be altered by stacking sequence and crystalline behavior, resulting a decrease in quantity of layers and an development in electrochemical parameters such as electron transport ability and band gap [37]. As a result, monolayer WS_2 synthesis is garnering increasing attention today in order to maximize all of the features of WS_2-related devices. Chemical vapor deposition (CVD), mechanical exfoliation, chemical exfoliation, and liquid exfoliation can all be used to make WS_2 nanosheets that are similar to graphene sheets. Among these approaches, the CVD technique can produce high-quality WS_2 nanolayers. CVD is a known technique for producing cost effective 2D TMD single layers [38]. According to Cong [39], single-step sulfurization of WO_3 results in the creation of monolayer WS2. Another study employed a controlled thermal reduction sulfurization technique to synthesize single and multiole layer WS_2. However, the necessity for specialized equipment and a high temperature

prevents it from being used commercially. Another acceptable method is mechanical exfoliation, however its inability to control the thickness and lateral size of nanoflakes limits its use in WS_2 exfoliation. Zhou used saltassisted CVD to create high-quality 2D TMDs [40]. They described the synthesis of 47 chemicals, including WS_2 single crystals at low temperatures (750–850 °C). Jin used a three-step procedure to make WS_2 [41]. The sulphur and metal sources were hydrogen sulphide (H_2S) and sodium tungstate, respectively, which were generated via the breakdown of sodium sulphate. Intercalation of Lithium (Li) into chemical exfoliation processes. The attractions among the layers are faded by the WS_2 layers. Following the ultrasonication, The WS_2 will be exfoliated into single or few layers during the intercalation stage. It should be dispersed in water. In comparison to the conversion of bulk WS_2 into MoS_2, the conversion of bulk WS_2 into nanosheets was hard Due to the resistance of the single layer, it was discovered to be significantly more challenging.WS_2 is working on intercalation. Miremadi and Morrison [42] in their book Ultrasonication was used to exfoliate WS_2 in 1988, and Li intercalation was used. Hydrolysis was then followed. This facilitates Li intercalation into the WS_2. The presence of hydrogen after water washing suggested the likelihood of additional exfoliation [43].

Table 1 Different materials used for gas permeation

S.NO	Polymer	Filler	Gas permeate reduction in %	References
1	Cellulose nanofibers	h-BN nanosheets	Oxygen gas permeate reduces up to 75.4% with 5% of loading	[34]
2	Epoxy resin	Boron nitride nanoplatelets	With 15 wt % of loading the water vapor permeate	[35]

			reduces up to 60%.	
3	Natural rubber (NR)	Surface functionalized graphene oxide (SGO)	With 0.3 wt% of SGO, 48% reduction in the air permeability occurs.	[36]
4	Low density polyethylene (LDPE)	clay nanocomposites	Oxygen permeability reduces up to 24% with 7% of clay.	[37]
5	PET	h-BN	With 10% wt O_2 permeability reduces to 95%	[38]
6	Polyethylenimine (PEI)	Reduced Graphene Oxide (RGO)	With 12.5 wt% of RGO H_2 Permeation reduces to 86%	[39],
7	Thermoplastic Polyurethane (TPU)	h-BN nanosheets	With 0.054 vol % of loading CO_2 permeation reduces up to 82%.	[40].
8	Acrylic Resin	Le-Hec Clay	With 9.1 wt% of loading, CO_2 permeation reduces to 93.8%	[41].

9	Polyvinyl alcohol (PVA)	MoS_2 nanosheets	With 2 wt% of loading H_2 permeation was reduces to 94%	[42]

2.4. Liquid Phase Exfoliation

Alternatively, liquid exfoliation looks to be a viable method for producing largigh-concentration WS_2 nanosheets in a quick, low-cost, and environmentally friendly manner. Furthermore, employing programmed sequential sonication and centrifuging stages, solvent-assisted exfoliation allows for precise control of nanoflakes thickness and size. Yuan et al. [44] described a simple one pot synthesis process for multilayer WS_2 nanosheets that are soluble in water , using sonication. They used liquid exfoliation in water and ultrasonication to make polyacrylic acid (PAA) modified WS_2 nanosheet from bulk WS_2. The nanosheets synthesized were able to adsorb DNA molecules, allowing them to be used in biosensing. Exfoliated WS_2 nanosheets can be used in a wide range of applications. One of the most prominent applications is as an electrocatalyst in hydrogen evolution processes (HER). Han et al. used a liquid exfoliation process in Dimethyl formamide (DMF) with the help of sonication and used the resulting sheets in HER. Jha et al. [45] used sonication to make humidity sensors out of liquid exfoliated WS_2 nanosheets in a 2-propanol and acetone combination. When exfoliated WS_2 was utilised as a catalyst, Koyyada et al. [46] found that it produced one point seven one times more H than bulk WS_2. Water molecules reduced van der Waal connections between layers in this case, and DMSO molecules aided exfoliation. Jung and colleagues [47] used liquid exfoliation in water to exfoliate MoS_2 and WS_2 before surface functionalization with 2-Mercaptoethanol. In N-methyl pyrrolidone, 1-vinyl-3-(3-aminopropyl)-imidazolium bromide (VAPimBr) ionic liquid was used as an auxiliary agent for WS_2 exfoliation [48]. Because of the relation of Sulphur with gold, combining tungsten disulfide nanosheet with hollow gold spheres (HGNs) resulted in the production of a WS_2/HGNs nanocomposite. Bhandavat and colleagues [49] used an acid treatment approach utilizing chlorosulfonic

acid to create surface functionalized few layer WS_2. Ultrasonication aided exfoliation(chemical) in $NaNO_3$/HCl yielded WS_2 and MoS_2 with yields of 52 and 58 percent, respectively [50]. Typically, liquid exfoliated nanosheets are mixed with suitable polymers to create polymer nanocomposites. Composites could potentially be made using a simple technique involving direct exfoliation of components in polymers. Vega-Mayoral and colleagues [51] investigated the effects of poly (vinyl alcohol) (PVA) on WS_2 exfoliation. Recent research has shown that combining sonication and grinding processes can result in a higher yield of TMD monolayers with fewer flaws. This idea was grasped by Paolucci et al. [52], who used sonicated and ball milling to generate WS_2 nanosheets that may be used in humidity sensing. WS_2 was exfoliated by Dai et al. using a combo of sonication with ball mill process with sodium dodecyl sulphate surfactant. LPE is considered as a good technique for tungsten disulfide exfoliation due to its advantages over other techniques. Despite this, low yield from these approaches remains a major issue. Intercalation or oxidation at borders of bulk TMDs have recently been used to alleviate this problem .[53] Xu et al. [54] used the modified LPE approach to pre-intercalate Li in WS_2 layers and got a yield of 18–22%. In photocatalytic hydrogen evolution events, the resulting nanosheets possess co-catalytic properties.

2.5. WS_2 and nanocomposites

In recent years, polymer nanocomposites have attracted a lot of attention. A number of studies involving polymer nanocomposites for the development of high-performance materials have been published [55-58]. The synergistic impact of filler and matrix can be used to generate great materials with increased or novel properties by incorporating nanoparticles into the polymer. Nanofillers can improve barrier property, strength, thermal, mechanical qualities as per recent research [59-61]. Layered materials like graphene, boron nitride, and TMDs have recently dominated the polymer nanocomposite field [62, 63]. MoS_2 reinforced polymer nanocomposites with a 2D structure have also been reported [58, 64-66]. However, two dimensional structured nanocomposites (polymer and nanofiller) based on WS_2 are uncommon, and IFWS_2 was often employed for reinforcing polymers. This makes IF-WS_2 materials a good solid lubricant for lowering friction and increasing polymer toughness. [67, 68]

2.6. PET

PET with an intrinsic viscosity of 0.81 dL/g was used. Nanocomposites were prepared using melt compounding technique in a twin-screw compounder with various wt.% of clay, 68.8% reduction in O_2 permeation for 5wt.% composite was reported, whereas 1wt.% showed 22.6% reduction and 3wt.% showed 14.2% respectively. They concluded that higher reduction in permeability of 1wt.% organoclay as compared to 3wt.% was due to the higher and better exfoliation at lower clay percentages [69].PET nanocomposites were prepared using two organoclays namely Cloisite 15A and Nanolin DK2 via melt blending technique, and were tested for their permeability with different weight percentages , among all compositions, 1wt.% of Nanolin/PET composite showed the highest reduction in permeability with 44.8%, whereas 2wt.% Cloisite/PET composite showed the superior barrier properties of all Cloisite/PET composites with 29.59% decrease in O_2 permeation as compared to the bottle grade PET. Furthermore, in their final remarks, they inferred that higher the degree of exfoliation, lower is the permeability and lower the wt. % of clay, higher is the exfoliation [70].

PET/Na^+MMT composites were synthesized by means of esterification clay addition (ES clay addition) and polycondensation (PC) clay addition (PC clay addition), better results in permeation with lower percentage composites of PET/Na^+MMT in ES clay addition method was observed as contrast to PC method due to better exfoliation and dispersion of clay in former, and a highest of 36 % reduction in oxygen permeability with 0.5wt.% PET/Na^+MMT composite was achieved [71].PET/PEN composite were prepared with 50/50 composition using ultrasonically aided extrusion and Oxygen permeation at different ultrasonic amplitudes varying from (0-10) μm was noted. 40% reduction in O_2 permeability coefficient at 0 μm amplitude was observed and it was concluded that ultrasonication had no effect on 50/50 PET/PEN composite [72].PET/MXD6/Clay(D72T) composites were synthesized using 4 methods and their barrier properties were observed: a blend of PET/MXD6 having a weight ratio of 9:1 was used as a polymer matrix. PET/MXD6 blend was found to have a 25.4% lower O_2 permeability constant than pure PET owing to the superior gas barrier properties of MXD6, addition of 3.5wt.% clay resulted in the further reduction of permeability constant by 10-20%. An overall 40-45% reduction in permeability constant was achieved using different wt.% of PET/MXD6/Clay

composite. It was concluded that when PET-clay is extruded first and followed by MXD6 addition, the clay is more homogeneously distributed and intercalated among two polymer phases (PET & MXD6) and the permeability constant is at lowest [73].

PET/MMT composites were formed using melt blending technique with 5wt.% MMT and a comparative study of PET nanocomposite versus nanocomposites of biopolymers was performed. OTR test at 0%RH (Relative Humidity) for the 5wt.% PET/MMT yielded a 55% reduction in O_2 permeability, and a 35% reduction at 80% RH for the same nanocomposite compared to pure PET, it was also reported that a Nano-bio composite blend of PHB/PCL had exhibited better oxygen, water and limonene barrier properties than pure PET. However, 5wt.%PET nanocomposite was observed to have the lowest permeability of all the nanocomposites[74]. PET/Na-MMT nanocomposite with different compositions were prepared using melt blending technique and it was found that oxygen permeation reduction increased until 2wt.% with the highest reduction of 52% and decreased when the wt.% was further increased, 5wt.% showed only 37% decrease, which could have been due to the presence of tactoid structures as suggested by the authors. In 0.5, 1 and 2 wt.% composites the clay was better exfoliated, whereas in 3 and 5 wt.% composites, clay was partially exfoliated and partially intercalated, which might have been the reason for their inferior O_2 barrier properties [75].

Recent years have seen a growing interest in using graphite derivatives due to their extremely high aspect ratios, in contrast to organoclays, graphene nanosheets have 25-130 times high gas barrier properties [76]. PET/FGO and PET/GO nanocomposites were synthesized using solution blending. GO was prepared using Hummers process and it was functionalized via nucleophilic substitution using alkyl bromide to convert the hydrophilic groups such as hydroxyl, epoxy and carboxylic acid to alkyl and alkyl ether. A 38% reduction in permeation of O_2 with 1wt.% PET/GO composite and 97% reduction with 3wt.% PET/FGO composite as compared to pure PET was achieved, greater reduction in FGO composites was reported to be due to homogeneous dispersion of graphene in PET [77]. PET/GNP(Graphite Nanoplatelets) nanocomposites of different compositions were prepared using melt compounding, and it was reported that the composites prepared via quenching had a lower degree of crystallinity and it was also observed that the oxygen

permeability is reduced by the presence of GNP and by the degree of crystallinity. 99% reduction in O_2 permeation using 1.5wt% was also claimed, the highest so far [78].PET/Cloisite 30B nanocomposites were prepared with varying wt.%, using in-situ polymerization and a highest of 50% reduction in O_2 permeation with 3wt.% composite was achieved [79]. PET/GO nanocomposites at low loadings (0.1-0.5wt%) were prepared by in-situ polymerization and it was noted that the PET nanocomposites had oxygen barrier properties superior by a factor of 2-3.3 as compared to pristine PET, a highest of 69.6% reduction in O_2 permeation with 0.5wt.% nanocomposite was reported [80].

PET/H-BN nanocomposites were synthesized using melt processing and a 42% reduction in O_2 permeability with 0.017vol% composite and 70% reduction with 3vol% composite was observed. At lower compositions the composites were observed to be almost as transparent as pure PET, with 0.057vol% composite having a transmittance of 85% whereas that of pure PET is 86%, however, with the increase in percentage of BNNS a steady decrease in transmittance was seen with 60% transmittance at 1vol% of BNNS, which is lower when compared with Graphene sheets, where only 0.02vol% resulted in 50% reduction in transmittance, the reason was reported to be the large band gap of BN, due to which the light is not absorbed in the visible region. BN was thus found to be a very attractive candidate for enhancing the gas barrier properties of PET without affecting its appearance, it was concluded that higher reduction can be achieved by using BN sheets of higher aspect ratio, and also by better alignment of sheets in polymer matrix [81].

PET nanocomposites with 2wt.%modified organoclays were prepared, clays were modified with oleic acid with the idea of combing both passive and active barrier properties, a good adhesion between clay and PET resulted in enhanced gas barrier properties, for PET/ ol-MMT and PET/ol-30B, a 54% and 74% decrease in OTR was reported [82]. PET nanocomposites using organo modified clay with compatibilizer (sulfonated polyester ionomer) were synthesized and a better intercalation and exfoliation in composites containing compatibilizer was reported. Compatibilizer improved the dispersion of clay, 50% reduction in CO_2 permeation was achieved with the composite containing 5wt.% clay and 1:1 mass ratio of compatibilizer and o-Mt [83]. PET/H-BN nanocomposites with various compositions varying from 1-10wt.% were prepared via in-

situ polymerization, 95% reduction in oxygen permeability for 10wt.% composite was claimed [84]. Despite of all the research explained earlier, (Table 2) also represents the effect of nanofillers and synthesis techniques on gas barrier properties.

Table 2 Effect of nano fillers and synthesis techniques on gas barrier properties of PET polymer

Polymer	**IV (dL/g)**	**Filler**	**Fraction**	**%Reduction in Permeability**	**Technique**	**Authors**
PET	0.81	DK2	1wt.% 3 wt.% 5 wt.%	22.6(O_2) 14.2(O_2) 68.8(O_2)	Melt compounding	[69]
PET	0.82	Cloisite 15A	1 wt.% 2 wt.% 3 wt.%	19.7(O_2) 29.59(O_2) 16.1(O_2)	Melt blending	[70]
PET	0.82	Nanolin DK2	1 wt.% 2 wt.% 3 wt.%	44.8(O_2) 29.59(O_2) 30.49(O_2)	Melt blending	[70]
PET	-	ES Clay addition	0.5 wt.% 2 wt.%	36(O_2) 29(O_2)	In-Situ polymerization	[71]
PET	-	PC Clay Addition	0.6 wt.% 2 wt.%	31(O_2) 25(O_2)	In-Situ Polymerization	[71]
PET	0.74	PEN	50 wt.%	40(O_2)	Melt extrusion	[72]
PET	0.80	MXD6 Clay-MXD6	10 wt.% (3.5/10) wt.%	25.4(O_2) 41.31(O_2)	Melt extrusion	[73]
PET	-	MMT	5 wt.%	55(0% RH) (O_2) 35(80%RH) (O_2)	Melt Blending	[74]

PET	0.84	Na-MMT	0.5 wt.% 1 wt.% 2 wt.% 3 wt.% 5 wt.%	28.7(O_2) 41.4(O_2) 51.7(O_2) 40.2(O_2) 36.8(O_2)	Melt Blending	[75]
PET	0.80	GNP	0.1 wt.% 0.5 wt.% 1 wt.% 1.5 wt.%	-0.9(O_2) -18(O_2) 75.6(O_2) 99(O_2)	Melt Compounding	[78]
PET	-	GO	1 wt.%	38.19(O_2)	Solution Blending	[77]
PET	-	FGO	1 wt.% 3 wt.%	85.18(O_2) 97.36(O_2)	Solution Blending	[77]
PET	0.71	Cloisite 30B	2 wt.% 3 wt.% 5 wt.%	25(O_2) 50(O_2) 12.5(O_2)	In-situ Polymerization	[79]
PET	0.536	GO	0.1 wt.% 0.3 wt.% 0.5 wt.%	51.23(O_2) 61.72(O_2) 69.9(O_2)	In-situ Polymerization	[80]
PET	0.8	H-BN	0.017vol% 3Vol%	42(O_2) 70(O_2)	Melt Processing	[81]
PET	0.84	ol-MMT ol-30B	2 wt.% 2 wt.%	54(O_2) 74(O_2)	Melt Processing	[82]
PET	0.78-0.84	o-Mt	5 wt.%	50(CO_2)	Melt Processing	[83]
PET	-	H-BN	10 wt.%	95%(O_2)	In-Situ Polymerization	[84]

Chapter 3

Materials & Methods

3.1. Materials Used

N-methyl-2-Pyrrolidone (NMP) was purchased from Sigma Aldrich and bilk Tungsten disulfide was purchased from local vendor. Industrial grade PET Poly(ethyleneterephthalate) with intrinsic viscosity of (0.81 dL/g) was provided by ECOPACK LTD.

3.2. Nanosheets Synthesis

300 mg of Tungsten disulfide powder mixed with 40mL of NMP in a 250mL capacity metallic cylinder was sonicated for 48hrs using a 120hertz fixed frequency sonicator at 60amplitude with a 1sec on and 1 sec off pulse in a cooled water bath. Resultant solution contained exfoliated nanosheets of varying aspect ratio, centrifugation at 1000rpm was applied for their separation, supernatant obtained in centrifuge tubes was collected and vacuum filtered on a PTFE membrane of 0.4um pore size to get rid of the excess NMP, filtrate containing membrane was then placed inside oven at 60^{o}C overnight to obtain the desired nanosheets, same procedure was then repeated at 750 and 500rpms. Nanosheets were characterized using XRD.

Figure 4 Nanosheets Synthesis

3.3. Nanocomposite film Synthesis

Composites were fabricated using 1000, 750 and 500rpm WSNS. PET membranes, pure and nanocomposites were synthesized using TIPS (temperature induced phase separation). PET pellets were dissolved in NMP at a temperature higher than its T_g (>165^{o}C) with constant magnetic stirring (200rpm) inside a 10ml black cap glass vial. Solution concentration was set at 550mg/10mL. Pellets were seen to be completely dissolved in 35-45 mins, nanosheets of desired concentration were then added and solution was further stirred magnetically on hot plate for further 15-20mins to ensure uniform dispersion of nanosheets inside polymer matrix, however, the color of solution was seen to shift from transparent to dark yellow brownish with time. Polymer chain disassociation and acetaldehyde formation while heating could be the possible reason for this occurrence [85]. Afterwards, solution was casted with great care in a 3in glass petri dish placed in oven at elevated temperature. Membranes with 50-150μm thickness were formed as soon as the solvent had evaporated. PET nanocomposite samples ranging from .0025-.02 wt% were fabricated and tested for CO_2 permeation. Membranes were seen to be extremely sensitive to evaporation time and evaporation temperature, with a little delay or earliness in opening of oven resulting in either a brittle or a membrane with patterns.

3.3.1. Parameters for optimization of PET membrane synthesis

3.3.1.1. Temperature for evaporation.

Optimization of temperature for PET membrane synthesis could be separated into two sections: A- Above glass crystallization temperature (**Tg**) and B- Below (**Tg**). **Tg** for PET is 67^{o}C for amorphous and 81^{o}C for crystalline PET. Here in this research PET polymer used was semi-crystalline as observed and shown in XRD analysis, therefore its **Tg** lies somewhere between 67-81^{o}C. PET films formed above **Tg** in 100-130^{o}C range were brittle with enhanced strength than below **Tg** films but still unsuitable for permeation testing. Films formed in the region of 130-150^{o}C range depicted enhanced strength. As the temperature was increased further, strength of membranes increased but with improved brittleness. In addition, increase in temperature was also associated with decrease in pore size and its distribution and an increase in density of films. 145^{o}C was chosen to be the ideal and optimized temperature for PET film synthesis where strength, ductility, brittleness and pore size were optimum for permeation analysis. Furthermore, with increase in temperature the appearance of films went from white (100-120)^{o}C range to brownish color in (120-200)^{o}C range. All PET nanocomposite films were prepared at **145^{o}C** evaporation temperature. PET films formed below **Tg** were completely amorphous and fragile and not suitable for testing, they would break by slightest of contact with anything rigid.

3.3.1.2. Time of Evaporation

Evaporation time was optimized once the variable of evaporation temperature was fixed. The ideal time for 145^{o}C was found to be roughly (1hr-1hr5) minutes; if heated for even a minute longer, the film became too brittle to test and shattered at the least contact. It was also discovered that every 10^{o}C increase in evaporation temperature resulted in a 10min reduction in evaporation time.

3.3.1.3. PET concentration

PET films were made at concentrations ranging from 300 mg/mL to 550 mg/mL of PET. PET films with concentrations ranging from 300 mg/mL to 500 mg/mL were found to be

too thin to be tested for penetration. After that, all PET nanocomposite films were made with a 550mg/mL concentration and thicknesses ranging from 70 to 110um.

3.3.1.4. Stirring RPM and stirring time effect.

The non-uniform dispersion of WS_2NS was considered to be the origin of strange patches on the surface of preliminary PET film samples produced. The stirring duration and rpm for the dissolution stage were modified to resolve the non-uniformity of the PET film's surface. Stirring duration was changed from 30 minutes to 1 hour while keeping the rpm constant at 500, and it was shown that 1 hour was the best stirring time for dissolution since it reduced non-uniformity to a large amount. Any further increase in stirring time would cause the PET, NMP, and WSNS mixture to turn brownish, which would be unappealing. rpm was changed while all other factors remained constant to better enhance the aesthetics of the PET film surface. The dissolution time increased as the rpm values increased because PET pellets rose in a glass vial and were farther away from the heating plate surface, taking longer to dissolve, whereas at 100rpm PET pellets were on the bottom of the glass vial and thus closer to the heating surface, taking less time to dissolve. Because rpm affects the stirring duration, the indirect negative effect was reduced by maintaining the rpm value constant at 100. Even after optimizing these two variables, there was still some non-uniformity on the surface of the PET film.

3.3.1.6. Casting Position effect inside oven

After failing to notice a considerable improvement in the aesthetics of the film's surface, it was considered that the problem was due to non-uniform heating and solvent evaporation. To address this issue, the casting position inside the ovens was optimized. In two different ovens, PET films were cast in 15 distinct places. It was discovered that one's position had a major impact on aesthetics. All the ovens had a distinct position where uniform heating and, as a result, uniform evaporation occurred, and these positions were not in the middle. This pattern was optimized, and all the spots that occurred from uneven heating were removed. Even after adjusting the casting positions, some patterns on the surface of the films remained.

3.3.1.7. Effect of Lid of the glass vial

This variable was the most difficult to predict having any effect on the film's surface appearance of all the factors examined. All non-uniform patterns vanished from films that were cast with the dissolution stage performed without the lid of the glass vial. The cause of this peculiar phenomena is that when the solvent evaporates during the dissolving phase with the lid intact, it condenses on the inner surface of the lid due to temperature differences. The condensed solvent then returns to the bulk mixture, implying that at any point during the dissolving process, there was a lower temperature in the bulk NMP than the remainder of the bulk temperature. The cooler NMP took longer to evaporate than the rest of the NMP when the lid was removed and the liquid was cast on a petri dish inside the oven, resulting in patterns on the surface. By removing the lid during the dissolution process, the problem of patterns was eventually solved. Table 3 contains the final optimized all variables.

Table 3 Optimized Variables

Temperature of Evaporation	**Time of Evaporation**	**Concentration**	**Stirring time**	**RPM**	**Lid**
145ºC	1hr	550mg/mL	1hr	100	None

3.4. Characterization

3.4.1. Working principle of Gas Permeation Testing System

In a gas permeation test system, we find out the permeability of the gases through the membrane. Permeability is the measure of the ability of a fluid to pass through a porous media. The permeability co-efficient, P, is defined as:

$$P = J\frac{\Delta l}{\Delta P}$$

$$where\ P = permeability\ co - efficient\ of\ the\ gas\ through\ membrane$$

$$J = \frac{volumetric\ flow\ rate}{area\ of\ membrane}\ , called\ volumtric\ flux\ of\ the\ fluid$$

$$\Delta l = Thickness\ of\ the\ membrane$$

$$\Delta P = pressure\ difference\ across\ the\ membrane$$

Moreover, the permeation of various gases through the same membrane, can be used to find the selectivity of one particular gas over another. The selectivity α_{AB} of gas A over gas B is found by the following equation:

$$\alpha_{AB} = \frac{P_A}{P_B}$$

For single gas permeation testing, a stainless-steel gas permeation rig is used. The gas permeation rig is used for testing the permeance of gases through a membrane. The membrane is fitted into the membrane cell. Feed gas is introduced at the top of the cell while permeate is exited from the bottom of the cell. For the purpose of finding out the flow rate of permeate gas, a portion of that gas is taken through a bubble flow meter, in which the time taken for the bubble to flow a fixed volume gives us the gas flow rate. The schematic diagram of the gas permeation rig is shown in (Figure 5).

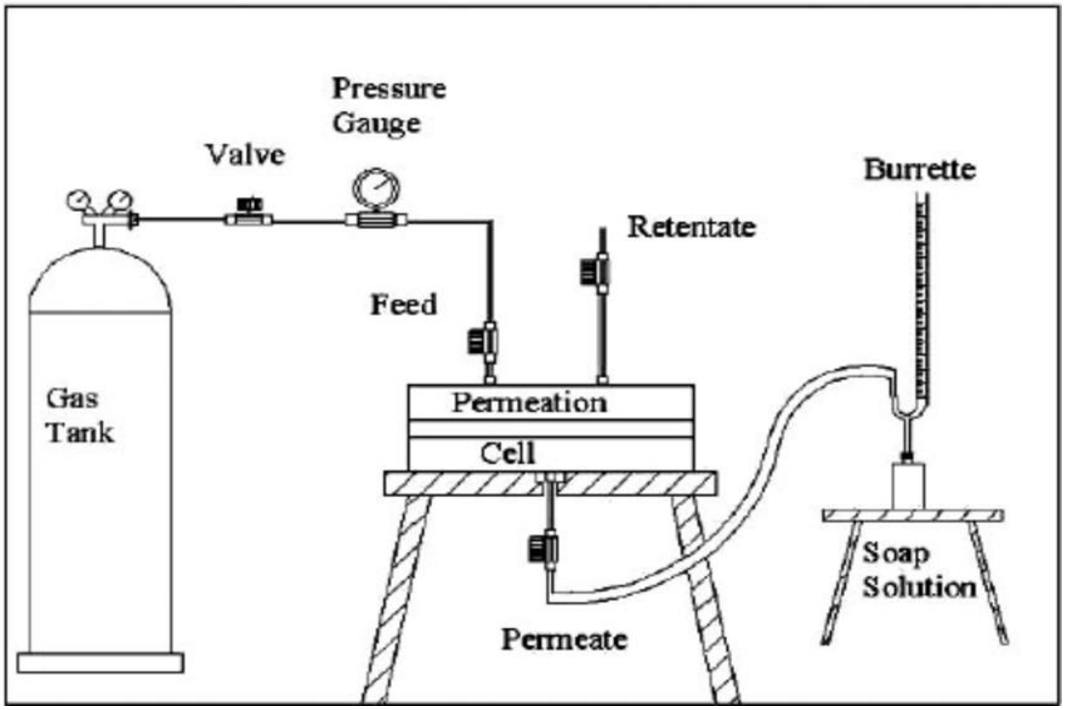

Figure 5 Schematic diagram of gas permeability testing system.

For the purpose of single gas permeability testing, we have used the PHILOS Gas Permeability Test System which has stainless steel gas permeation rig in it. The films were tested for permeation of CO_2 and O_2 gases at 3 bar gauge pressure

3.4.2. Working principle of SEM

The science behind the process of scanning electron microscopy (SEM) is the interaction of electrons with specimen material. When an electron beam is introduced into a column of the Scanning Electron Microscope, it does not encounter any atoms of any gas or liquid, in the atmosphere because a vacuum is established in that column. There is no interaction of electrons with matter, until it encounters the highly dense solid material. When the electron beam is incident on a sample, it transfers some of its energy to the molecules in the sample. This causes it to be reflected at an angle to its original well-defined trajectory. This results in the formation of back-scattered electrons, secondary electrons and X-rays. These interactions give us much needed information about the topography, composition, crystal structure and the presence of any electrical and magnetic fields. All these

interactions result in the scattering of electrons, which can be classified into two main types, elastic and inelastic scattering, as shown in (Figure 6).

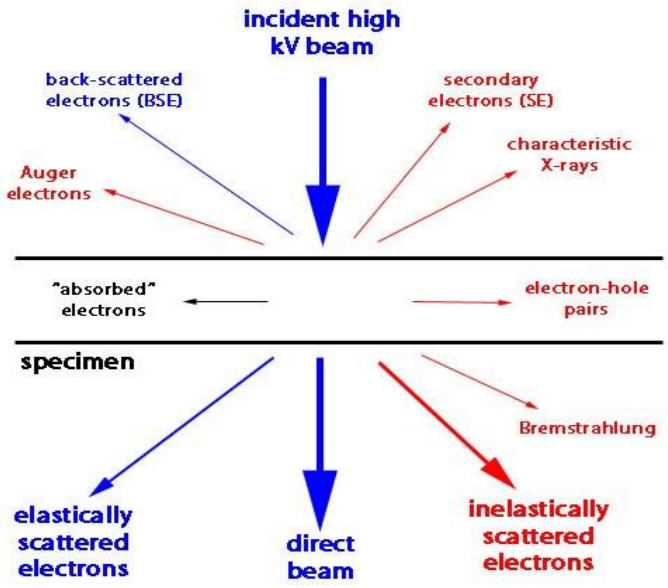

Figure 6 Scattering of electrons on interaction with matter.

Scanning Electron Microscopy (SEM) is used to study the morphology of membranes. It can also be used to study the presence and distribution of pores throughout the membrane. For this purpose, electrons are produced by an electron gun, passed through accelerating voltage which causes them to travel quickly down a column, through many lenses and apertures, The lenses and apertures are used to produce a focused beam of electrons which ultimately hits the sample. The sample is placed in the chamber area. As the electrons are supposed to be focused onto the sample, therefore both the column and the sample chamber must be under vacuum, which can be brought about by a series of pumps. The beam is focused on to a particular area of the material by using scan coils, located directly above the objective lens. The scanning of the electron beam over that region of the sample, helps us in studying the properties of a particular portion of the sample. Different signals are given out from this process which are then captured and analyzed by suitable detectors. The main components of the Scanning Electron Microscope (SEM) are:

- Electron source

- Column and electromagnetic lenses
- Electron detector
- Sample chamber
- Display screen

The schematics of the Scanning Electron Microscope can be shown as follows.

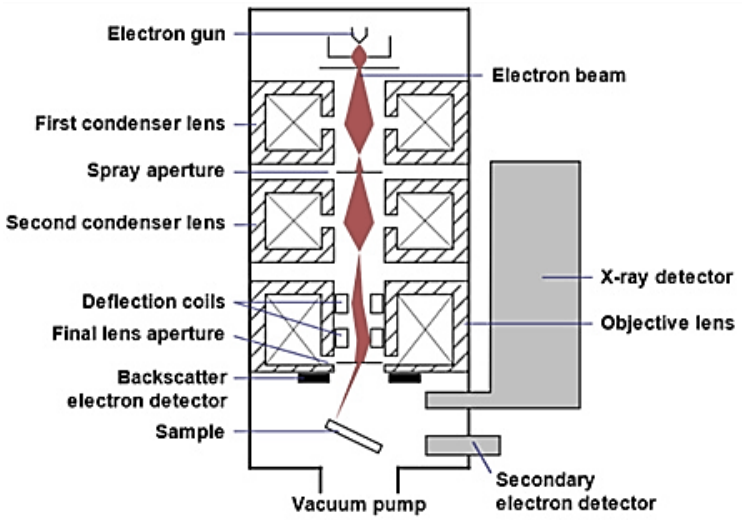

Figure 7 Schematic diagram of Scanning Electron Microscope

SEM analysis is performed by using TESCAN MAIA3 Field Emission Scanning Electron Microscopy (FESEM) for determining the morphological properties of the membrane samples. All the membrane samples having .005%, .010%, .015%, 0.25%, 0.050% and 0.075% w/w (filler-to-polymer) PET/BNNS films were characterized using this arrangement for the study of their pore distribution and pore structure. The analyses are performed at an accelerating voltage of 2 kV and magnifications of 5000x, 10,000x, 15,000x, 20,000x, 25,000x and 30,000x. The final SEM images were then studied to determine their surface features.

3.4.3. Working principle of AFM

An AFM uses a cantilever with a very sharp tip to scan over a sample surface. As the tip approaches the surface, the close-range, attractive force between the surface and the tip cause the cantilever to deflect towards the surface. However, as the cantilever is brought even closer to the surface, such that the tip makes contact with it, increasingly repulsive force takes over and causes the cantilever to deflect away from the surface. A laser beam is used to detect cantilever deflections towards or away from the surface. By reflecting an incident beam off the flat top of the cantilever, any cantilever deflection will cause slight changes in the direction of the reflected beam. A position sensitive photo diode (PSPD) can be used to track these changes. Thus, if an AFM tip passes over a raised surface feature, the resulting cantilever deflection and the subsequent change in direction of reflected beam is recorded by the PSPD.

An AFM images the topography of a sample surface by scanning the cantilever over a region of interest. The raised and lowered features on the sample surface influence the deflection of the cantilever, which is monitored by the PSPD. By using a feedback loop to control the height of the tip above the surface-thus maintaining constant laser position-the AFM can generate an accurate topographic map of the surface features.

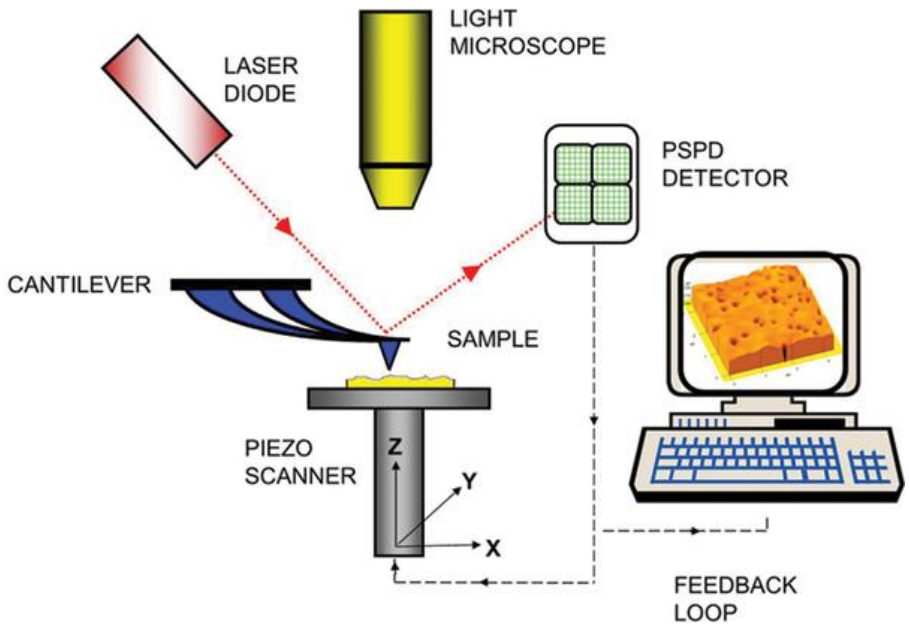

Figure 8 Schematic of AFM

If we summarize the characterization techniques, following figure can be helpful. First of all permeation of membranes can be tested and verified through gas permeation rig. Then after AFM technique is applied for WSNS nanosheets to study different dimensions and analytical measurements. After getting to know about all the analytical measurements of nanosheets, SEM technique is used for the study of morphology. SEM can easily verify the porosity and tortuosity of the polymer membrane.

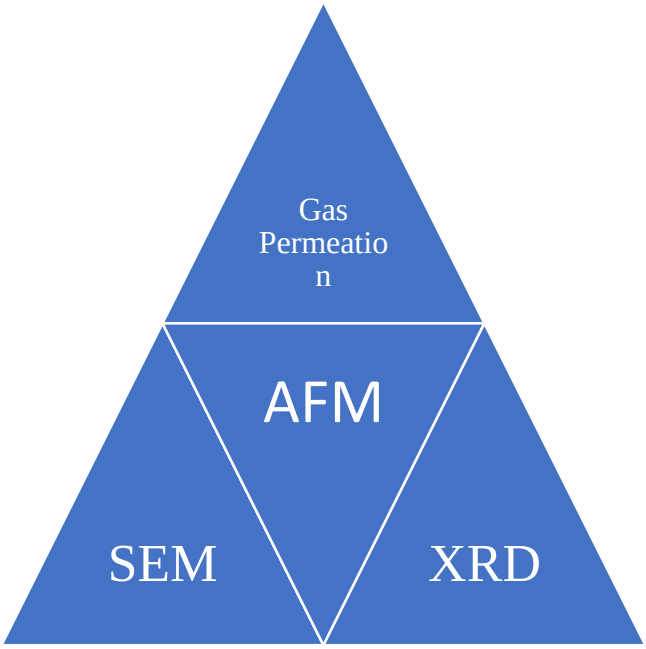

Figure 9 Characterization Techniques

Chapter 4

Results & Discussions

Through SEM and AFM, the dimensions of WSNS were characterized. SEM was used to evaluate the morphology of nanocomposites, XRD were used to observe the type of interaction between WSNS and PET.

4.1. Permeation Models

Single gas permeation testing was done on all of the polymer nanocomposite films with 0%, 0.0025%, 0.005%, 0.01%, 0.02%, 0.03%, and 0.04% WSNS. The permeation tests were done on a gas permeation rig that was part of the PHILOS Gas Permeability Testing System. At 3 bar, the amount of CO_2 that could pass through the films was calculated. Samples were only tested at 3bar because the pressure of CO_2 inside carbonated bottles is almost 3bar, or 2.7bar. All of the samples showed no selectivity. This means that the plot in Figure 10 shows the permeation of CO_2.

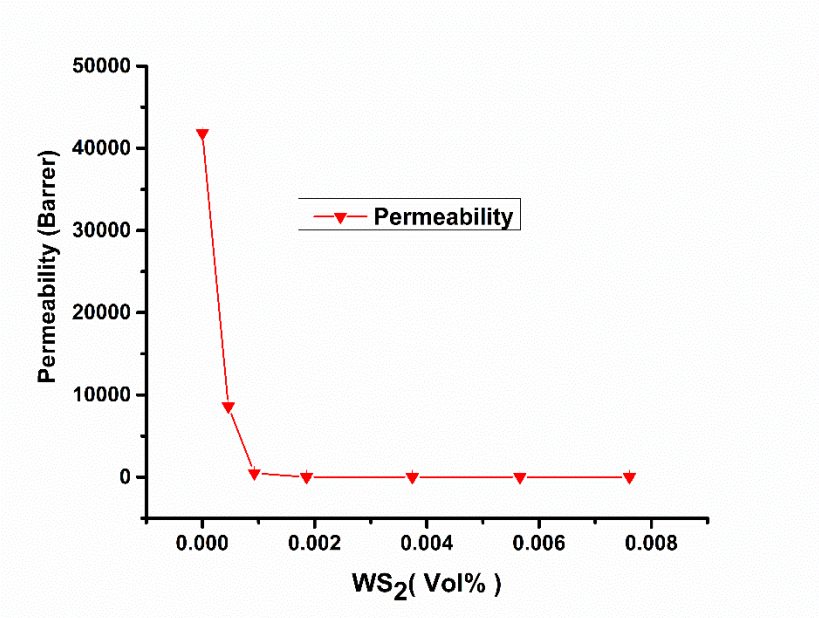

Figure 10 Effect of volume fraction of filler on permeability

There was 41826.71922 Barrer permeation in a sample film with no filler, but only 8594.512439

Barrer permeation in a sample with 0.0025 percent filler. That's a 79.4521

percent drop in permeation compared to the sample with no filler. In the same way, permeation decreased with increasing filler loading until a 0.01 percent sample showed no permeation for 11 hours. Samples with.01 percent,.02 percent,.03 percent, and.04 percent filler loading were tested for 11 hours. It goes without saying that if the films had been tested for longer, there would have been some permeation and the results would have been different. The permeation results, on the other hand, show very clearly how well WSNS work to stop gas from getting through the polymer. Samples from.001 percent to.04 percent were made because SEM results showed that even at.005 percent, the structure was semiporous and neither gas could get through for 11 hours. (Table 4) also shows the results of the permeation test.

Table 4 Experimental Permeation Results

Amount of Filler	**Pressure (bar)**	**Permeation (Barrer)**	**%Reduction in Permeation**
0.0025	3	8594.512439	79.4521
0.005	3	481.8438054	98.848
0.01	3	0	100
0.02	3	0	100
0.03	3	0	100
0.04	3	0	100

4.2. Permeation Models

The predictions of the model were based on an aspect ratio of 2500. From the curve fittings, we can tell that the Cussler model is close to the experimental values. The reason could be that the Cussler model takes into account that aspect ratio and volumer fraction have a bigger effect on tortuosity and, as a result, lessen permeation than other models. For the highest loading composite, Cussler's model predicts that permeation will

drop 8 times more than Nielsen's model. Different S values were also tried out with the Bhardawaj model. The Gusev and Lusti model was also used to figure out the current numbers, and the results were similar to Nielsen's. Comparisons of models with this work have been shown in (Figures 11). It was clear that the reduction in permeation that could be seen in experiments was more than what the theoretical models had predicted. Permeation tests were done for 11 hours for CO_2. Since the films were not selective CO_2 results were plotted. Because the models don't take time into account, the actual results are better than what the theories say they should be.

4.2.1. Gusev and Lusti Model:

The model works for random scattering of discs that don't touch each other. Picard et al. used the coefficient values of β =0.71 and xo=3.47 to get results for nylon-6/montmorillonite composites that were similar to those of the Nielsen model. For this prediction, the same values were used [86]. 2500 was taken as the aspect ratio.

$$\frac{Kcomposite}{Kmatrix} = \exp[-\left(\frac{\alpha\emptyset}{xo}\right)^{\beta}]$$

Table 5 Gusev & Lusti model Variables

Wt%	Vol% (∅)	Aspect Ratio (α)	Relative Permeability (theoretical)	Permeability (Barrer)	Relative Permeability (Experimental)
0	0	2500	1	41826.71922	1
0.0025	0.00046094	2500	0.633064	8594.512439	0.205479
0.005	0.000923769	2500	0.472862	481.8438054	0.01152
0.01	0.001855138	2500	0.292669	0	0
0.02	0.003741054	2500	0.132422	0	0
0.03	0.005658521	2500	0.06639	0	0
0.04	0.007608336	2500	0.0352	0	0

4.2.2. Bharadwaj Model

This model considers the effect of orientation of nanofillers on permeation. In incorporates S factor, for perpendicular orientation S=1 and the model reduce to Nielsen model. Aspect ratio was again taken to be 2500. Using Bharadwaj model orientation can also be predicted

$$\frac{Kcomposite}{Kmatrix} = \frac{1-\emptyset}{1+\frac{L}{2W}\emptyset\frac{2}{3}\left(S+\frac{1}{2}\right)} \quad (4.3)$$

$$S=\frac{1}{2}(3\cos^2\Theta-1) \quad (4.4)$$

4.2.3. Nielsen Model

Nielsen model takes in to account the effect of volume fraction $\emptyset$ and aspect ratio α. Orientation of nanofiller to the gas flow is assumed to be perpendicular and their dispersion to be uniform. Criteria for this model application is $\emptyset \ll 10\%$ & $\alpha\emptyset \ll 1$. Aspect ratio as determined in dimensional analysis of WSNS is taken to be 2500. From (Figure 11**)** it can be observed that the experimental values deviate greatly from the Nielsen model predicted values because the criteria $(\alpha\emptyset \ll 1)$ is not fulfilled as shown in (Table 6)

$$\frac{Kcomposite}{Kmatrix} = \frac{1-\emptyset}{1+\frac{\alpha}{2}\emptyset} \quad (4.1)$$

Table 6 Nielson Model Variables

Wt%	**Vol% (∅)**	**Aspect Ratio (α)**	**Relative Permeability (theoretical)**	**Permeability (Barrer)**	**Relative Permeability (Experimental)**	**Criteria $\alpha\emptyset \ll 1$**
0	0	2500	1	41826.71922	1	0
0.0025	0.00046094	2500	0.634154715	8594.512439	0.205479	1.152350796
0.005	0.000923769	2500	0.463670593	481.8438054	0.01152	2.309422444
0.01	0.001855138	2500	0.300743657	0	0	4.637844814
0.02	0.003741054	2500	0.175511491	0	0	9.352635003

0.03	0.005658521	2500	0.12316647	0	0	14.14630146
0.04	0.007608336	2500	0.09441979	0	0	19.02084022

4.2.4. Cussler Model

Cussler model assumes the dispersion of nanofillers inside polymer matrix to be uniform, and nanofiller orientation to be perpendicular to the flow. Aspect ratio was taken to be 2500. The model is mostly applicable to lower loadings and sets the criteria as $\emptyset \ll 1\ \%$ & $\alpha\emptyset \gg 1$. As seen in (Table 7) the criterion is fulfilled, due to which Cussler model fits closely to our experimental results.

$$\frac{Kcomposite}{Kmatrix} = \left(1 + \frac{\alpha^2\emptyset^2}{1-\emptyset}\right)^{-1} \qquad (4.2)$$

Table 7 Cussler Model Variables

Wt%	**Vol% (∅)**	**Aspect Ratio (α)**	**Relative Permeability (theoretical)**	**Permeability (Barrer)**	**Relative Permeability (Experimental)**	**Criteria $\alpha\emptyset \ll 1$**
0	0	2500	1	41826.71922	1	0
0.0025	0.00046094	2500	0.429456466	8594.512439	0.205479	1.152350796
0.005	0.000923769	2500	0.157769432	481.8438054	0.01152	2.309422444
0.01	0.001855138	2500	0.04434672	0	0	4.637844814
0.02	0.003741054	2500	0.01126123	0	0	9.352635003
0.03	0.005658521	2500	0.004944213	0	0	14.14630146
0.04	0.07608336	2500	0.002735483	0	0	19.02084022

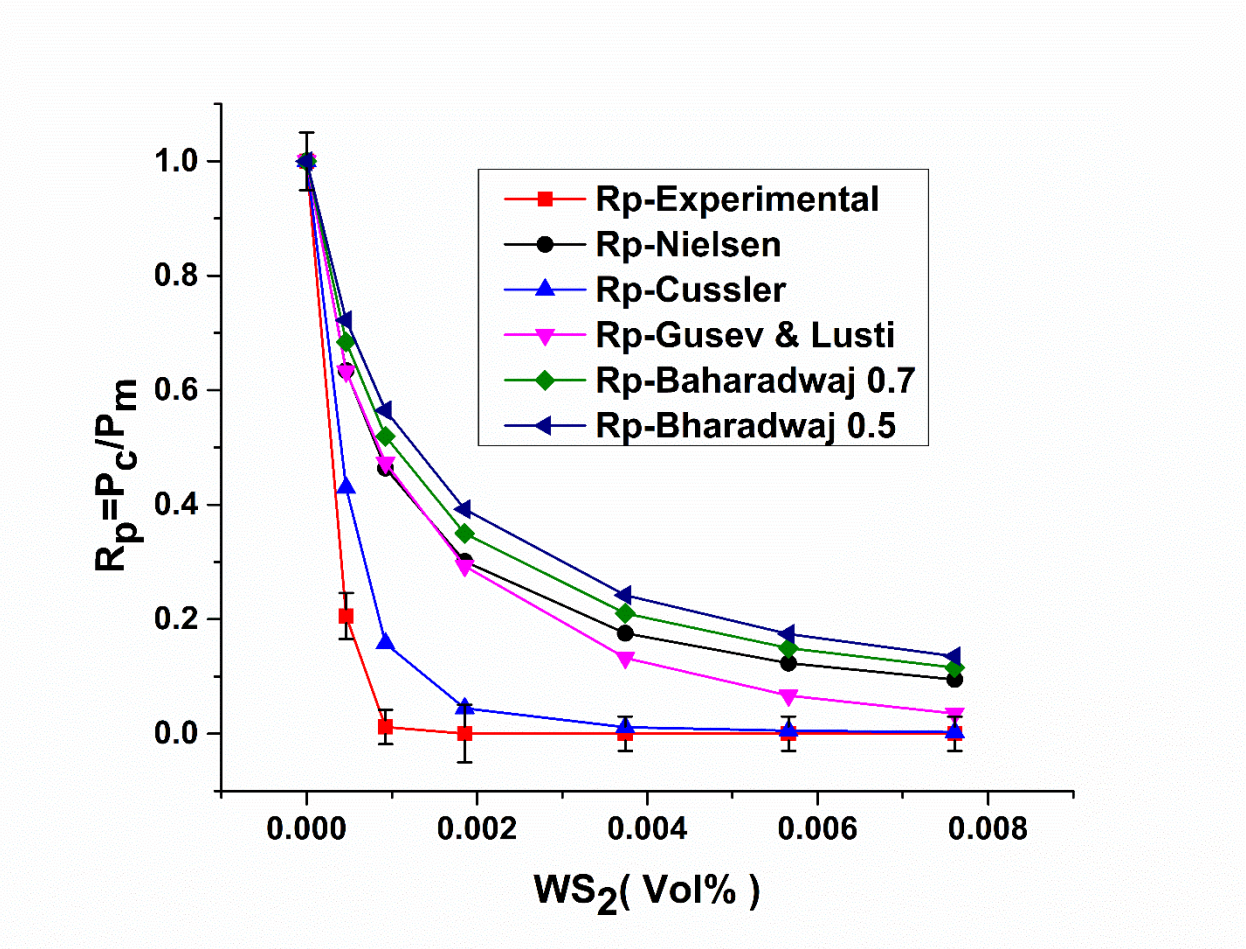

Figure 11 Nielsen, Cussler, Bharadwaj, Gusev and Lusti Models combined comparison with experimental permeation results

4.3. Analysis of dimensions for WSNS

AFM and SEM were utilised in order to measure the dimensions of the nanosheets. These bulk WS_2 powder SEM images were taken at 20,000 and 30,000 magnifications, which demonstrates very clearly that they are not exfoliated at this stage. These images can be found in (Figure 12). A structure resembling a stack can be seen. When compared to (Figure 13), it is crystal clear that the Few layer WSNS have been exfoliated successfully. SEM images of the WSNS were taken at the same magnifications as those of the bulk material in order to clearly check the conversion of the bulk material into nanosheets.

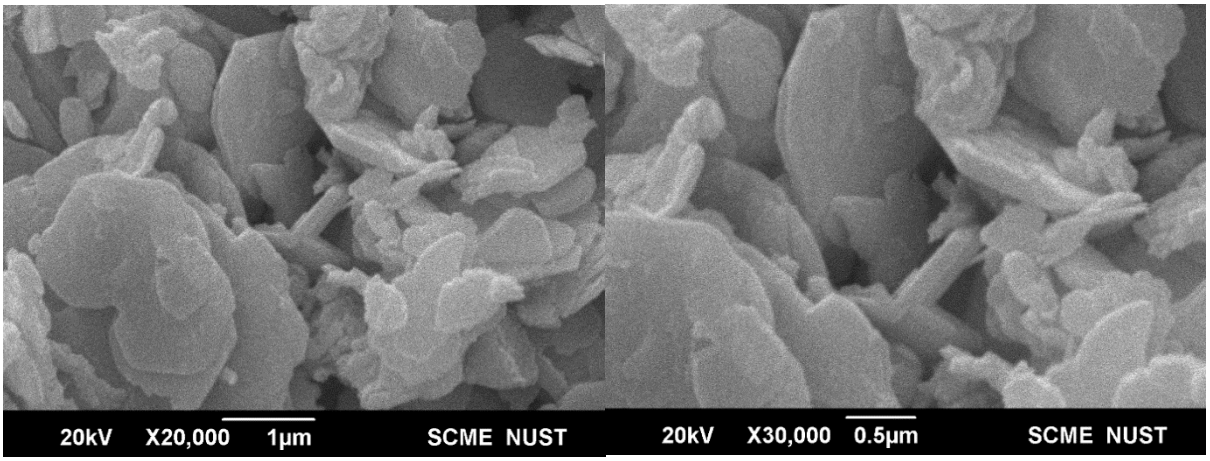

Figure 12 SEM Images of bulk WS_2 at 20000 and 30000 magnification

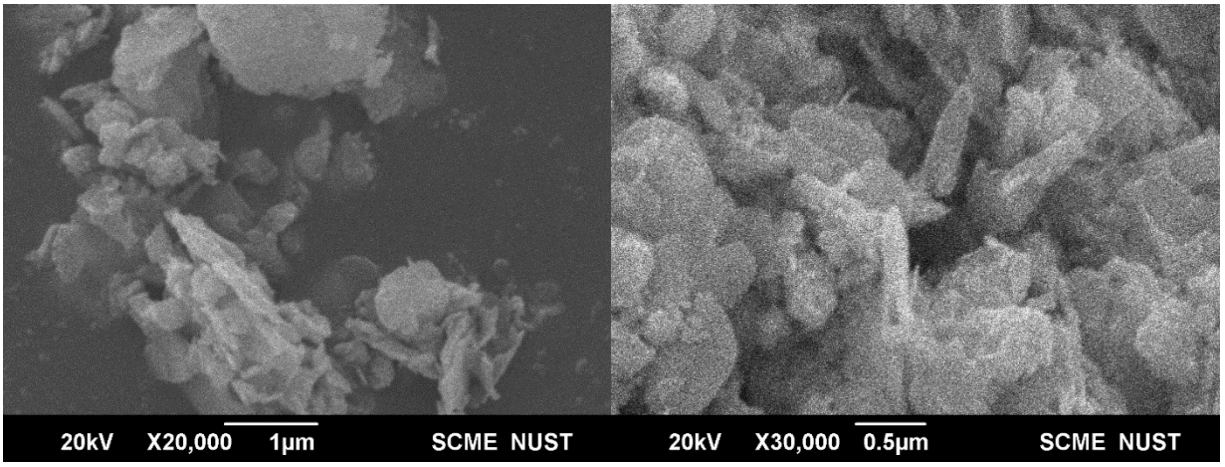

Figure 13 SEM o WS_2 Nanosheets at 20000 and 30000 magnification

The AFM histogram suggests that the average thickness of nanosheets is approximately 1.79 millimeters

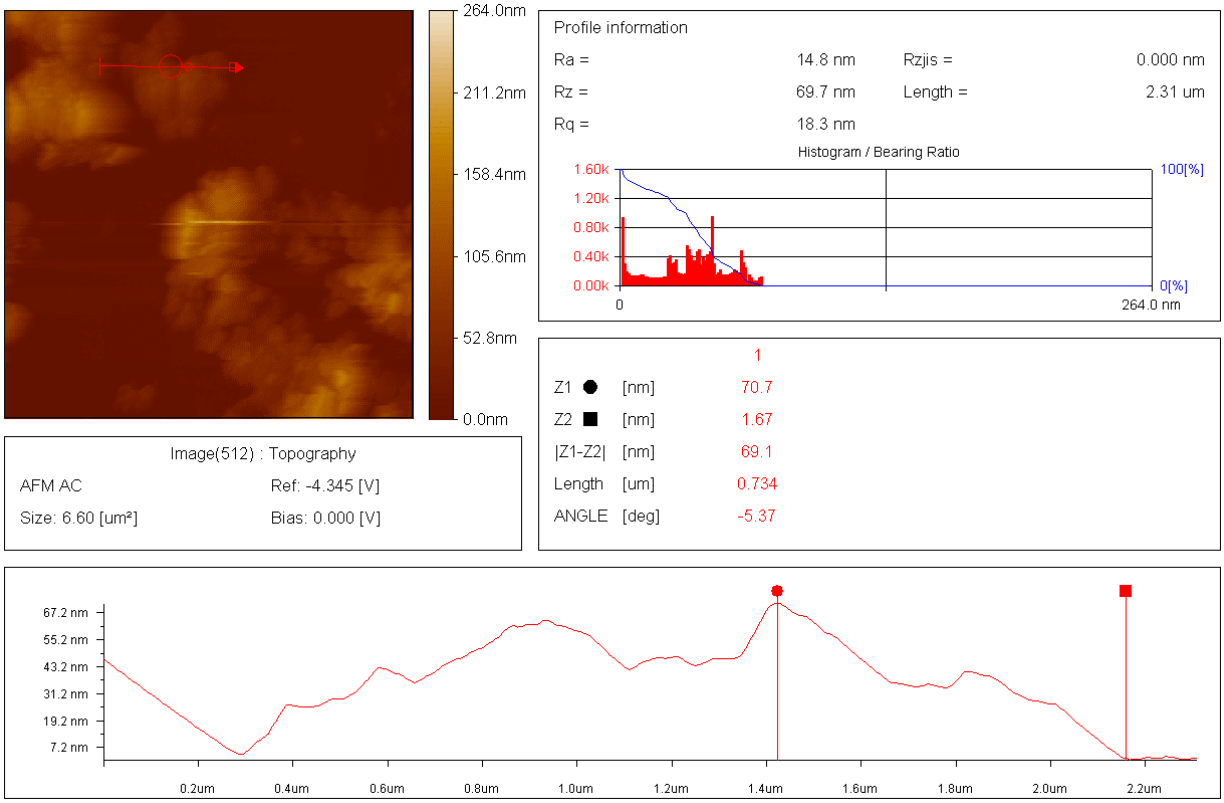

Figure 14 AFM histogram of WS_2 Nanosheets

4.4. SEM

All of the film samples, to varying degrees, exhibited a morphological pattern that depicted a porous top surface and a dense bottom surface. A rough evaporation/top surface stature was seen through apparent observation, whereas the bottom surface had shinny optics.

4.4.1. Rough/Top

When the concentration of nanosheets is increased, a striking transformation in morphology can be observed. The decrease in pore size and its distribution can be observed in 0.025wt percent composite relative to pure PET film, which indicates the successful execution of nanosheets inculcation. The same trend follows in all of the higher

concentration composites, with 0.01wt percent composite exhibiting an almost perfect dense structure dev. At first glance, 0.02 weight percent of the composite appears to contain pores; however, upon closer inspection, it was discovered that the structures in question were cavities, not pores (Figure 20-21). It goes without saying that the change in morphologies displayed by samples with nanosheets concentration is quite remarkable when taking into account the amount of nanosheets that was used. It is also important to note that there is almost no visible evidence of nanosheets on the surface, and the reason for this could be due to the extremely low amount of nanosheets that are used.

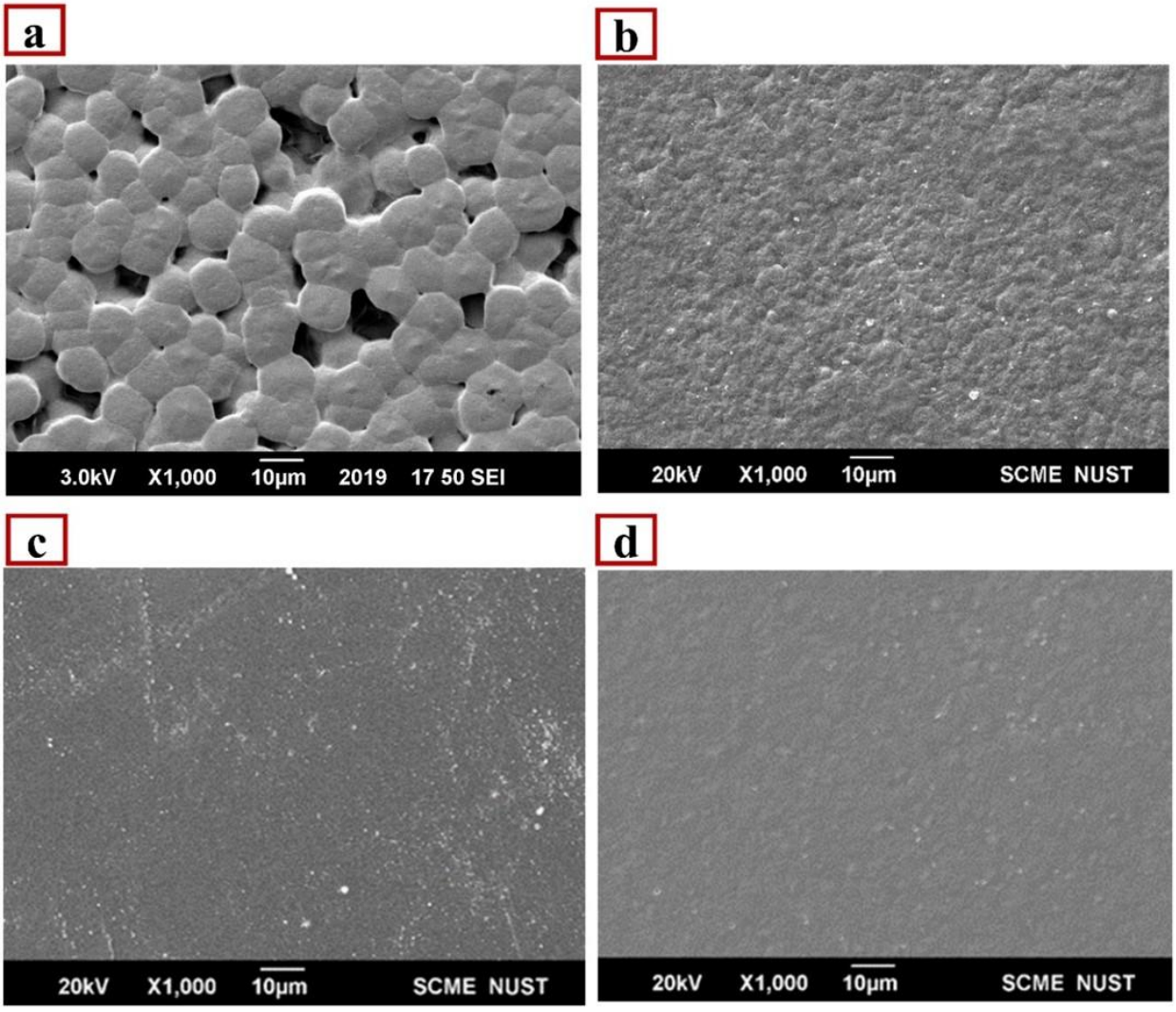

Figure 15 SEM Surface Images (a)Pure PET (b) 0.0025 wt% (c) 0.005 wt % (d) 0.01 wt%

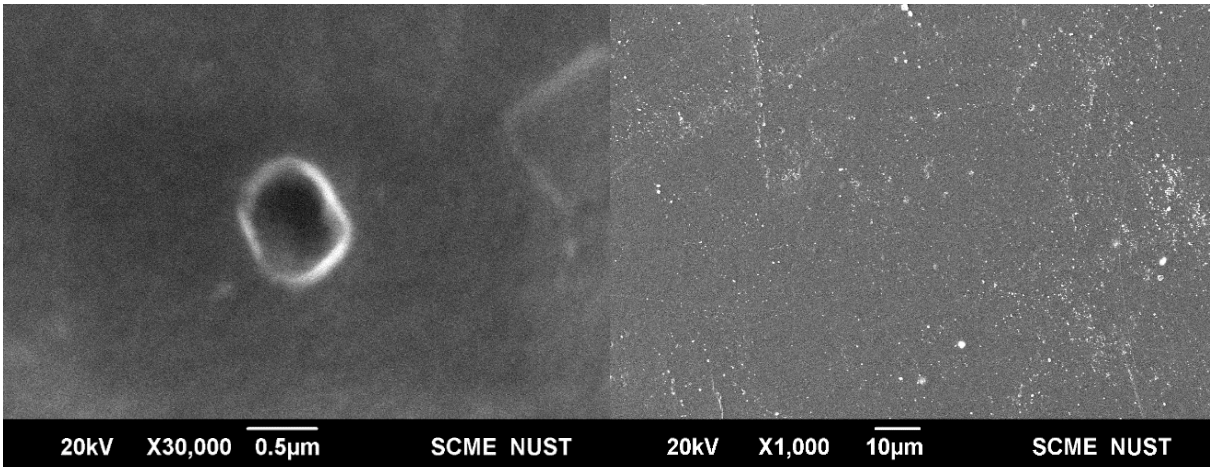

Figure 16 SEM Surface Images, 0.01 wt% zoom in and 0.002 w%

4.4.2 Cross-Section

Obtained SEM cross-section images that are immediately understandable and don't require any explanation (Figure 19-20). There is a discernible shift in the orientation of the polymeric chains in the Pure film as one moves from the top to the bottom, and one can see a pattern very similar to this in the composites with a higher weight percent. The pure sample appears to be packed tightly together, with little space separating the chains; however, from the middle to the top of the cross-section, the chains look slightly tangled, and there are large pores and voids in this portion. The structure of the material is semi-dense at 0.0025 weight percent. The 0.01 weight percent sample reveals an almost ideal dense bottom structure beneath it. The drying process during membrane fabrication leaves gaps, which the polymer fills to a large extent but not completely, which is why there are pores visible in the Pure sample.

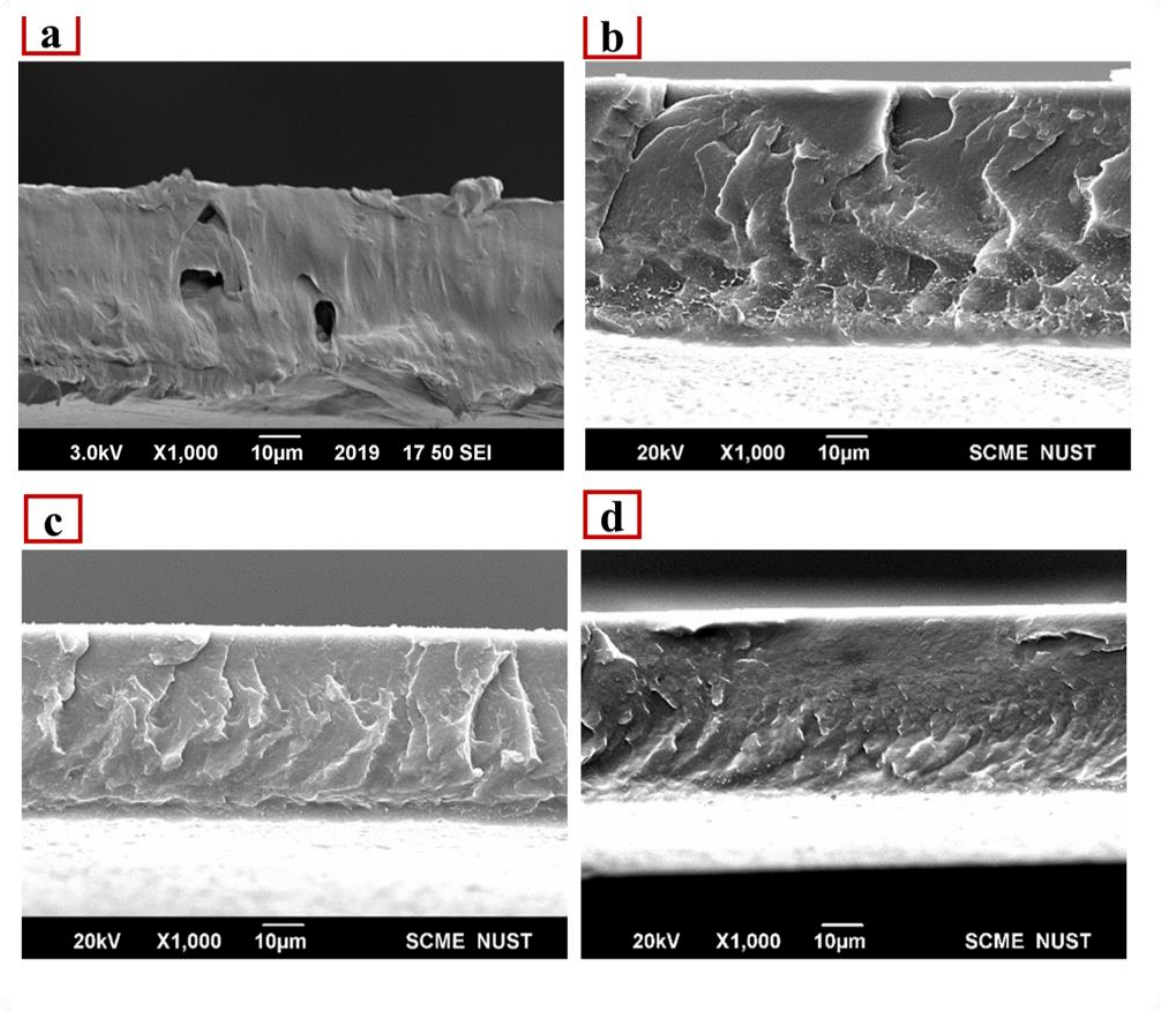

Figure 17 SEM Cross Section Images (a)Pure PET (b) 0.0025 wt% (c) 0.005 wt% (d) 0.01 wt%

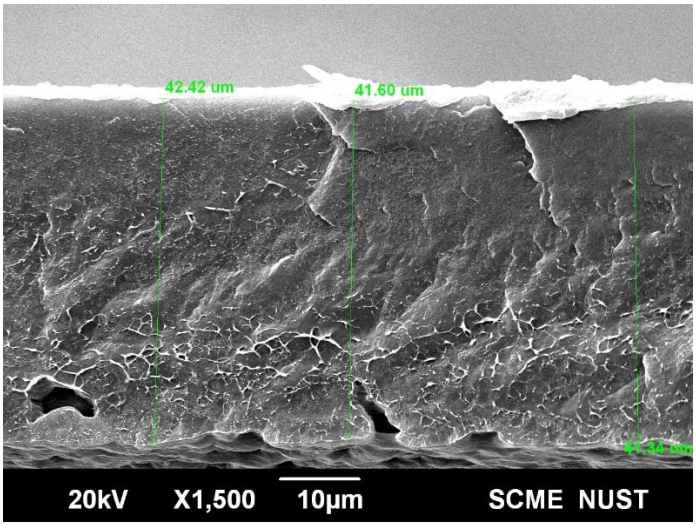

Figure 18 0.02wt%-Cross-Section

It was determined that films have an asymmetrical nature by using SEM on cross sections of films. Moving from a shiny, bottom surface to a rough, top surface causes films to become more porous. Additionally, an increase in weight percent was seen to cause the dense side to become denser, as well as the porous, rough side, which was also seen to become denser. After the solvent evaporates, the gaps in the polymeric chains are primarily filled by the polymer itself as well as the remaining nanosheets, which results in a dense structure. This occurs after the gaps are left by the solvent. A very important point is needed to add here that it can be observed from SEM images of 0.01 weight percent and 0.02 weight percent, the film having 0.02 weight percent have good gas barrier property but it have changed the structure of the polymer. If image of 0.02 weight percent is observed from below it has some unusual cracks. So, we can conclude that 0.01 weight percent is critical point.

4.5. XRD

4.5.1 Nanosheets

The lower portion of Figure 21 displays an XRD pattern that shows crystalline, single-phase WS2 nanosheets that have a hexagonal crystal structure. There were no additional peaks found. X-ray patterns of bulk WS_2 powder have been provided so that they can be compared to the standard pattern obtained from WS_2 samples using XRD. (JCPDS Card No. 08-0237) The characteristic peaks of WS_2 nanosheets were found to be located at 33.2°, 39.89°, 44.51° and 58.3° respectively, which correspond to the (001), (103), (006) and (110) planes. Due to the fact that there is a peak at 14 degrees, it can be deduced that the nanostructures contain WS_2 multilayers [87].

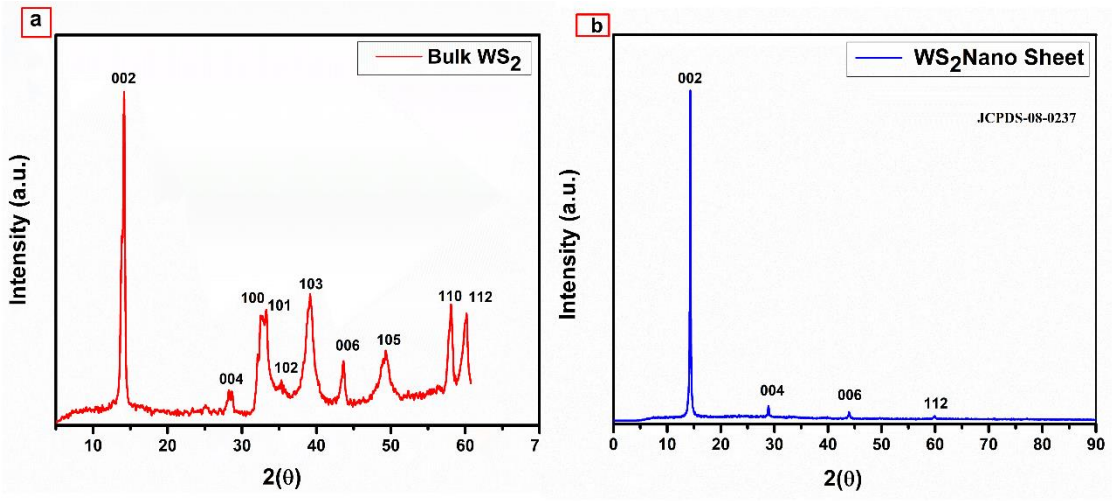

Figure 19 Comparison of XRD pattern of WS_2 bulk and WS_2 nanosheets

4.5.2. Nanocomposites

The XRD pattern of PET polymer is displayed in the Figure 22. The absence of sharp peaks in this region is powerful proof that the material possesses a polymeric behavior.

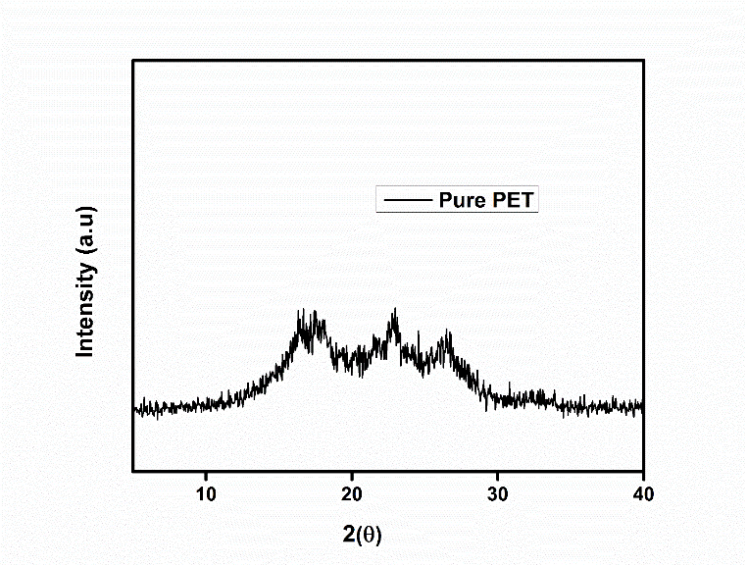

Figure 20 XRD pattern of Pure PET

In contrast to figure 22 the XRD of nanocomposites show sharp peaks after incorporation of WSNS nanosheets in Figure 23.

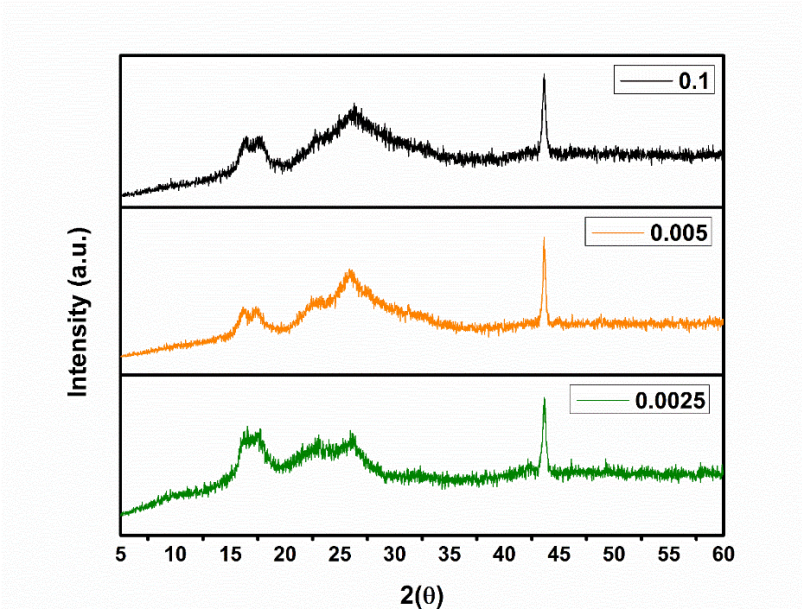

Figure 21 PET/WSNS nanocomposites XRD

According to the presence of peaks at 26.56 and 44.89, it was discovered that the samples studied had, to varying degrees, preserved their crystal structures. The polymer chain is loosened as a result of heat treatment at high temperatures, which causes the peaks in PET films without any filler loading to have the lowest peak intensities. In addition to the findings from the SEM, all of the composites exhibit an increase in crystallinity (Figure 23), which validates the role that nanosheets play in increasing chain entanglement, which in turn leads to an increase in crystallinity and a reduction in permeation. The findings from XRD and SEM on every single sample are consistent with one another. It was discovered that the h-interaction between WS_2 and polymer is purely physical, as there was no peak shift seen in any of the composites that were examined.

Conclusion

A superficial method was used for synthesis of tungsten Disulfide nanosheets know as solution processing. Nanocomposites were prepared by TIPS method and with a very tiny amount of filler loading results of gas barrier was quite remarkable due to proper dispersion. Contrast of theoretical models and experimental data, experimental results were close to Cussler model and even better permeation reduction because of 12 hours testing, results can be better if long time experiments are done. 98% permeation of CO_2 was reduced by only 0.05 weight percent sample. SEM results confirmed the dense surface which complement the permeation results. The findings from XRD and SEM on every single sample are consistent with one another. Increase in weight percent of filler can show good permeation results as in this study 0.02 weight percent exhibited good results but on other hand it changed the structure of polymer.

WSNS can be used in other field of sciences such as biomedical and biosensing etc. time of permeation can be increased from 11 hours to get more perfect results. The gas barrier capabilities of PET-WSNS films were evaluated over the duration of 11 hours, and the results were compared to theoretical models. It was discovered that the reduction in permeation observed in experiments exceeded the values predicted by the models. It has been suggested that the development of a permeation model that takes into account the variable of time will result in more accurate results. Centrifuge RPM effects the size of nanosheets so different values of RPM in future can be tried to get different variety of nanosheets. As a result of the fact that the pore size and its distribution in pure PET film can be controlled to a great degree of precision through the application of different temperatures,

References

[1] Profaizer, M. *Passive Barrier Assessment of PET Bottles through an FEM Simulation of Gas Permeability*. in *Excerpt from the Proceedings of the COMSOL Multiphysics User's Conference*. (2005). Citeseer.

[2] Wyeth, N. and R. Roseveare, *Biaxially oriented poly (ethylene terephthalate) bottle*. 1973, Google Patents.

[3] Boutroy, N., et al., *Hydrogenated amorphous carbon film coating of PET bottles for gas diffusion barriers.* (2006). **15**(4-8): p. 921-927.

[4] Kuzminova, A., et al. *Barrier coatings on polymeric foils for food packaging*. in *WDS*. (2013).

[5] Nakaya, M., et al., *Gas and flavor barrier thin film coating to plastic closures.* (2018). **4**(1): p. 1-17.

[6] Beeva, D., et al., *Controlling the barrier properties of polyethylene terephthalate. A review.* (2015). **42**(7): p. 45-52.

[7] Rex, W.J. and D.J. Tennant, *Polymeric linear terephthalic esters*. 1949, Google Patents.

[8] WorldEconomicForum, *World Economic Forum, Ellen MacArthur Foundation and McKinsey & Company, The New Plastics Economy Rthinking The Future of Plastics.* 2016.

[9] Boutroy, N., et al., *Hydrogenated amorphous carbon film coating of PET bottles for gas diffusion barriers.* (2006). **15**: p. 921-927.

[10] Kazminova, A., et al. *Barrier coatings on polymeric foils for food packaging*. in *Proceedings of the 22nd Annual Conference of Doctoral Students—WDS*. (2013).

[11] Nakaya, M., A. Uedono, and A. Hotta, *Recent progress in gas barrier thin film coatings on PET bottles in food and beverage applications.* Coatings, (2015). **5**(4): p. 987-1001.

[12] Kanishka Bhunia, Hongchao Zhang, and Shyam S Sablani, *Gas Barrier Packaging.* Reference Module in Food Sciences, (2016).

[13] Beeva, D., et al., *Controlling the barrier properties of polyethylene terephthalate. A review.* (2015). **42**(7).

[14] Profaizer, M. *Passive Barrier Assessment of PET Bottles through an FEM*. in *COMSOL Multiphysics User's Conference*. (2005). Stockholm.

[15] Nakaya, M., et al., *Gas and flavor barrier thin film coating to plastic closures.* Quarterly Physics Review, (2018). **4**(1): p. 1-17.

[16] Naz, R., *STORAGE IN POLYETHYLENE TEREPHTHALATE BOTTLES: CHANGES AND SHELF LIFE.* Fruit Juices, (2018).

[17] Zahid, M., et al., *Graphene morphology effect on the gas barrier, mechanical and thermal properties of thermoplastic polyurethane.* Compos Sci Technol, (2020). **200**: p. 108461.

[18] Zhang, J., et al., *2D nanomaterials for tissue engineering application.* Nano Res., (2020). **13**(8): p. 2019-2034.

[19] Murali, A., et al., *Emerging 2D nanomaterials for biomedical applications.* (2021).

[20] Tiwari, S.K., et al., *Graphene research and their outputs: Status and prospect.* J SCI-ADV MATER DEV (2020). **5**(1): p. 10-29.

[21] Telkhozhayeva, M., et al., *Higher Ultrasonic Frequency Liquid Phase Exfoliation Leads to Larger and Monolayer to Few-Layer Flakes of 2D Layered Materials.* (2021). **37**(15): p. 4504-4514.

[22] Kilikevičius, S., et al., *Numerical investigation of the mechanical properties of a novel hybrid polymer composite reinforced with graphene and MXene nanosheets.* (2020). **174**: p. 109497.

[23] Lin, S., et al., *Liquid-phase exfoliation of violet phosphorus for electronic applications.* (2021).

[24] Hu, T., et al., *Two-dimensional nanomaterials: fascinating materials in biomedical field.* (2019). **64**(22): p. 1707-1727.

[25] Duan, J., et al., *Metal-organic framework nanosheets: An emerging family of multifunctional 2D materials.* (2019). **395**: p. 25-45.

[26] Azeem, M., et al., *Improving gas barrier properties with boron nitride nanosheets in polymer-composites.* (2019). **12**: p. 1535-1541.

[27] Adithya, S.P., et al., *Nanosheets-incorporated bio-composites containing natural and synthetic polymers/ceramics for bone tissue engineering.* (2020).

[28] Zhang, J., et al., *Improving the gas barrier, mechanical and thermal properties of poly (vinyl alcohol) with molybdenum disulfide nanosheets.* (2019). **57**(7): p. 406-414.

[29] Sharma, M.D., C. Mahala, and M.J.C. Basu, *AgPd alloy nanoparticles decorated MoS2 2D nanosheets: efficient hydrogen evolution catalyst in wide pH condition.* (2019). **4**(1): p. 378-386.

[30] Zhao, H., et al., *Structural defects in 2D MoS2 nanosheets and their roles in the adsorption of airborne elemental mercury.* (2019). **366**: p. 240-249.

[31] Li, Y., et al., *2D/2D/2D heterojunction of Ti3C2 MXene/MoS2 nanosheets/TiO2 nanosheets with exposed (001) facets toward enhanced photocatalytic hydrogen production activity.* (2019). **246**: p. 12-20.

[32] Yang, S. and K.J.J.o.M.S. Zhang, *Few-layers MoS2 nanosheets modified thin film composite nanofiltration membranes with improved separation performance.* (2020). **595**: p. 117526.

[33] Braga, D., et al., *Quantitative determination of the band gap of WS2 with ambipolar ionic liquid-gated transistors.* (2012). **12**(10): p. 5218-5223.

[34] Sethulekshmi, A., et al., *Insights into the reinforcibility and multifarious role of WS2 in polymer matrix.* (2021). **876**: p. 160107.

[35] Schutte, W., J. De Boer, and F.J.J.o.S.S.C. Jellinek, *Crystal structures of tungsten disulfide and diselenide.* (1987). **70**(2): p. 207-209.

[36] Radisavljevic, B., et al., *Single-layer MoS2 transistors.* (2011). **6**(3): p. 147-150.

[37] Chia, X., et al., *Electrochemistry of nanostructured layered transition-metal dichalcogenides.* (2015). **115**(21): p. 11941-11966.

[38] Lan, C., et al., *Wafer-scale synthesis of monolayer WS2 for high-performance flexible photodetectors by enhanced chemical vapor deposition.* (2018). **11**(6): p. 3371-3384.

[39] Cong, C., et al., *Synthesis and optical properties of large-area single-crystalline 2D semiconductor WS2 monolayer from chemical vapor deposition.* (2014). **2**(2): p. 131-136.

[40] Zhou, J., et al., *A library of atomically thin metal chalcogenides.* (2018). **556**(7701): p. 355-359.

[41] Jin, Y., et al., *Na2SO4-Regulated high-quality growth of transition metal dichalcogenides by controlling diffusion.* (2020). **32**(13): p. 5616-5625.

[42] Miremadi, B.K. and S.R.J.J.o.a.p. Morrison, *The intercalation and exfoliation of tungsten disulfide.* (1988). **63**(10): p. 4970-4974.

[43] Yang, D., R.J.J.o.P. Frindt, and C.o. Solids, *Li-intercalation and exfoliation of WS2.* (1996). **57**(6-8): p. 1113-1116.

[44] Yuan, Y., R. Li, and Z.J.A.c. Liu, *Establishing water-soluble layered WS2 nanosheet as a platform for biosensing.* (2014). **86**(7): p. 3610-3615.

[45] Jha, R.K. and P.K.J.N. Guha, *Liquid exfoliated pristine WS2 nanosheets for ultrasensitive and highly stable chemiresistive humidity sensors.* (2016). **27**(47): p. 475503.

[46] Koyyada, G., et al., *Enhanced solar light-driven photocatalytic degradation of pollutants and hydrogen evolution over exfoliated hexagonal WS2 platelets.* (2019). **109**: p. 246-254.

[47] Jung, D., et al., *Surface functionalization of liquid-phase exfoliated, two-dimensional MoS2 and WS2 nanosheets with 2-mercaptoethanol.* (2018). **18**(9): p. 6265-6269.

[48] Tan, Y., et al., *Ionic liquid auxiliary exfoliation of WS2 nanosheets and the enhanced effect of hollow gold nanospheres on their photoelectrochemical sensing towards human epididymis protein 4.* (2018). **262**: p. 982-990.

[49] Soares, D.M., S. Mukherjee, and G.J.C.A.E.J. Singh, *TMDs beyond MoS2 for electrochemical energy storage.* (2020). **26**(29): p. 6320-6341.

[50] Lin, H., et al., *Rapid and highly efficient chemical exfoliation of layered MoS2 and WS2.* (2017). **699**: p. 222-229.

[51] Vega-Mayoral, V., et al., *Photoluminescence from liquid-exfoliated WS2 monomers in poly (vinyl alcohol) polymer composites.* (2016). **26**(7): p. 1028-1039.

[52] Paolucci, V., et al., *Two-step exfoliation of WS2 for NO2, H2 and humidity sensing applications.* (2019). **9**(10): p. 1363.

[53] Jawaid, A., et al., *Redox exfoliation of layered transition metal dichalcogenides.* (2017). **11**(1): p. 635-646.

[54] Xu, D., et al., *High yield exfoliation of WS2 crystals into 1–2 layer semiconducting nanosheets and efficient photocatalytic hydrogen evolution from WS2/CdS nanorod composites.* (2018). **10**(3): p. 2810-2818.

[55] He, X., et al., *Thermal, antioxidant and swelling behaviour of transparent polyvinyl (alcohol) films in presence of hydrophobic citric acid-modified lignin nanoparticles.* (2019). **127**: p. 665-676.

[56] Matos, C.F., F. Galembeck, and A.J.J.C. Zarbin, *Multifunctional and environmentally friendly nanocomposites between natural rubber and graphene or graphene oxide.* (2014). **78**: p. 469-479.

[57] Asimakopoulos, I., G. Psarras, and L.J.E.P.L. Zoumpoulakis, *Barium titanate/polyester resin nanocomposites: Development, structure-properties relationship and energy storage capability.* (2014). **8**(9).

[58] Chen, P., et al., *Enhanced thermal and mechanical properties of PLA/MoS2 nanocomposites synthesized via the in-situ ring-opening polymerization.* (2018). **440**: p. 1143-1149.

[59] Moniruzzaman, M. and K.I.J.M. Winey, *Polymer nanocomposites containing carbon nanotubes.* (2006). **39**(16): p. 5194-5205.

[60] Pavlidou, S. and C.J.P.i.p.s. Papaspyrides, *A review on polymer–layered silicate nanocomposites.* (2008). **33**(12): p. 1119-1198.

[61] Rozenberg, B. and R.J.P.i.p.s. Tenne, *Polymer-assisted fabrication of nanoparticles and nanocomposites.* (2008). **33**(1): p. 40-112.

[62] Wang, T., et al., *Biosensor based on ultrasmall MoS2 nanoparticles for electrochemical detection of H2O2 released by cells at the nanomolar level.* (2013). **85**(21): p. 10289-10295.

[63] Zhang, D., et al., *Room temperature hydrogen gas sensor based on palladium decorated tin oxide/molybdenum disulfide ternary hybrid via hydrothermal route.* (2017). **242**: p. 15-24.

[64] Zhou, K., et al., *Preparation of poly (vinyl alcohol) nanocomposites with molybdenum disulfide (MoS 2): structural characteristics and markedly enhanced properties.* (2012). **2**(31): p. 11695-11703.

[65] Tsai, C.-Y., S.-Y. Lin, and H.-C.J.P. Tsai, *Butyl rubber nanocomposites with monolayer MoS2 additives: Structural characteristics, enhanced mechanical, and gas barrier properties.* (2018). **10**(3): p. 238.

[66] Madeshwaran, S., et al. *Mechanical and thermal properties of MoS2 reinforced epoxy nanocomposites*. in *Journal of Physics: Conference Series*. (2018). IOP Publishing.

[67] Simić, D., et al., *Inorganic fullerene-like IF-WS2/PVB nanocomposites of improved thermo-mechanical and tribological properties.* (2016). **184**: p. 335-344.

[68] Yang, H., et al., *Synthesis of inorganic fullerene-like WS2 nanoparticles and their lubricating performance.* (2006). **17**(5): p. 1512.

[69] Hamzehlou, S. and A. Katbab, *Bottle-to-bottle recycling of PET via nanostructure formation by melt intercalation in twin screw compounder: Improved thermal, barrier, and microbiological properties.* Journal of applied polymer science, (2007). **106**(2): p. 1375-1382.

[70] Frounchi, M. and A. Dourbash, *Oxygen barrier properties of poly (ethylene terephthalate) nanocomposite films.* J Macromolecular Materials Engineering, (2009). **294**(1): p. 68-74.

[71] Labde, R.K., *Preparation and characterization of polyethylene terephthalate/montmorillonite nanocomposites by in-situ polymerization method*. 2010, University of Toledo.

[72] Gunes, K., et al., *Fast in situ copolymerization of PET/PEN blends by ultrasonically-aided extrusion.* J Polymer, (2010). **51**(5): p. 1071-1081.

[73] Donadi, S., et al., *PET/PA nanocomposite blends with improved gas barrier properties: Effect of processing conditions.* Journal of applied polymer science, (2011). **122**(5): p. 3290-3297.

[74] Sanchez-Garcia, M., E. Gimenez, and J. Lagaron, *Novel PET nanocomposites of interest in food packaging applications and comparative barrier performance with biopolyester nanocomposites.* Journal of Plastic Film Sheeting, (2007). **23**(2): p. 133-148.

[75] Wang, Y. and S.A. Jabarin, *Novel preparation method for enhancing nanoparticle dispersion and barrier properties of poly (ethylene terephthalate) and poly (m-xylylene adipamide).* Journal of applied polymer science, (2013). **129**(3): p. 1455-1465.

[76] Cui, Y., et al., *Gas barrier properties of polymer/clay nanocomposites.* J RSC Advances, (2015). **5**(78): p. 63669-63690.

[77] Shim, S.H., et al., *Facile method to functionalize graphene oxide and its application to poly (ethylene terephthalate)/graphene composite.* ACS applied materials interfaces, (2012). **4**(8): p. 4184-4191.

[78] Al-Jabareen, A., et al., *Improving the oxygen barrier properties of polyethylene terephthalate by graphite nanoplatelets.* Journal of applied polymer science, (2013). **128**(3): p. 1534-1539.

[79] Esmaeilzadeh, A., et al., *Preparation and Characterization of Layered Silicate Polyethylene Terephthalate Nanocomposite by in Situ Polymerization.* Journal of Petroleum Science and Technology, (2016). **6**(2): p. 45-55.

[80] Szymczyk, A., et al., *Oxygen Barrier Properties and Melt Crystallization Behavior of Poly(ethylene terephthalate)/Graphene Oxide Nanocomposites.* Journal of Nanomaterials, (2015). **2015**: p. 10.

[81] Xie, S., et al., *Boron nitride nanosheets as barrier enhancing fillers in melt processed composites.* J Nanoscale, (2015). **7**(10): p. 4443-4450.

[82] Majdzadeh-Ardakani, K., et al., *A novel approach to improve the barrier properties of PET/clay nanocomposites.* International Journal of Polymer Science, (2017). **2017**.

[83] Vidotti, S.E., et al., *Effect of an organo-modified montmorillonite on the barrier properties of PET nanocomposites using a polyester ionomer as a compatibilizing agent.* J Materials Research, (2017). **20**(3): p. 826-834.

[84] Wilczak, W.A. and L.M. Nicholson, *Process for providing polymers comprising hexagonal boron nitride*. 2017, Google Patents.

[85] Lucchetta, G. and S.J.K.E.M. Chirico, *Acetaldehyde generation in processing PET by means of hot runner systems.* (2014).

[86] Picard, E., et al., *Barrier properties of nylon 6-montmorillonite nanocomposite membranes prepared by melt blending: influence of the clay content and dispersion state: consequences on modelling.* (2007). **292**(1-2): p. 133-144.

[87] Mahler, B., et al., *Colloidal synthesis of 1T-WS2 and 2H-WS2 nanosheets: applications for photocatalytic hydrogen evolution.* (2014). **136**(40): p. 14121-14127.